

## Supplementary Information for

# Bis(mesityl)phosphinic acid: Photo-Triggered Release of Metaphosphorous Acid in Solution

David E. Fast,<sup>a</sup> Michal Zalibera,<sup>ab</sup> Andrea Lauer,<sup>cd</sup> Anna Eibel,<sup>a</sup> Caroline Schweigert,<sup>e</sup> Anne-Marie Kelterer,<sup>a</sup> Martin Spichty,<sup>f</sup> Dmytro Neshchadin,<sup>a</sup> Dominik Voll,<sup>cd</sup> Hanna Ernst,<sup>e</sup> Yu Liang,<sup>e</sup> Kurt Dietliker,<sup>g</sup> Andreas N. Unterreiner,<sup>e</sup> Christopher Barner-Kowollik,<sup>cd</sup> Hansjörg Grützmacher<sup>g</sup> and Georg Gescheidt\*<sup>a</sup>

<sup>a</sup>*Institute of Physical and Theoretical Chemistry, NAWI Graz, Graz University of Technology, Stremayrgasse 9, 8010 Graz, Austria*

<sup>b</sup>*Institute of Physical Chemistry and Chemical Physics, Slovak University of Technology, Radlinskeho 9, 81227 Bratislava, Slovakia*

<sup>c</sup>*Preparative Macromolecular Chemistry, Institut für Technische Chemie und Polymerchemie, Karlsruhe Institute of Technology (KIT), Engesserstr. 18, 76128 Karlsruhe, Germany*

<sup>d</sup>*Institut für Biologische Grenzflächen (IBG), Karlsruhe Institute of Technology (KIT), Herrmann-von-Helmholtz-Platz 1, 76344 Eggenstein-Leopoldshafen, Germany*

<sup>e</sup>*Institute of Physical Chemistry, Karlsruhe Institute of Technology (KIT), Fritz-Haber-Weg 2, 76131 Karlsruhe, Germany*

<sup>f</sup>*Laboratory of Molecular and Cellular Biology, Structures and Interactions of Molecular Biosystems, Ecole Normale Supérieure de Lyon, 46, Allée d'Italie, 69364 Lyon, cedex 07, France*

<sup>g</sup>*Department of Chemistry and Applied Biosciences, ETH (Swiss Federal Institute of Technology), Vladimir-Prelog-Weg 1, Zurich, CH-8093, Switzerland*

\*E-Mail: g.gescheidt-demner@tugraz.at

## Table of Contents

1	Experimental .....	S3
2	TR EPR .....	S7
3	Calculations.....	S7
4	Polymerization Experiments .....	S15
4.1	PLP-ESI-MS of methyl methacrylate initiated by BAPO (1) and BAPO-OH (2) under bulk conditions .....	S15
4.2	PLP-ESI-MS of butyl acrylate (0.5 M in acetonitrile) initiated by BAPO (1) and BAPO-OH (2) .....	S20
4.3	<sup>1</sup> H CIDNP of BAPO (1) and BAPO-OH (2) in the presence of butyl acrylate (0.5 M in acetonitrile) .....	S23
4.4	Surfactant-free emulsion polymerization (SFEP) of methyl methacrylate initiated by BAPO-ONa (3).....	S24
5	Photolysis Experiments.....	S26
5.1	<sup>31</sup> P NMR of BAPO-OH (2) after photolysis.....	S26
5.2	ESI-MS of BAPO (1) and BAPO-OH (2) after photolysis .....	S27
6	Femtosecond Pump Probe Spectroscopy .....	S29
7	References.....	S33

# 1 Experimental

**Materials.** Bis(mesityl)phosphinic acid **2** was synthesized according to published procedures.<sup>S1,S2</sup> IRGACURE 819 (**1**) was purchased from BASF and used as received. Methyl methacrylate (MMA, Sigma-Aldrich, 99 %, stabilized) and butyl acrylate (BA, Fluka, purum,  $\geq 99.0$  %, stabilized) were freed from inhibitor by passing through a column of activated basic alumina (VWR). Sodium trifluoroacetate (Sigma-Aldrich, 98 %), tetrahydrofuran (THF, Scharlau, multisolvent GPC grade, 250 ppm BHT), methanol (Roth, HPLC grade) and acetonitrile (Roth, LC-MS grade) for ESI-MS measurements were used as received. Acetonitrile-*d*<sub>3</sub> (Euriso-top) and THF-*d*<sub>8</sub> (Ciba-Geigy) for NMR and CIDNP experiments were used as received. For the trapping experiments, ethanol (AustrAlco, 99.9 %, absolut) was passed through a column packed with 3A molecular sieves (Roth) under argon and distilled prior to use.

**Laser Flash Photolysis (LFP).** LFP experiments were performed with a LKS80 Laser Flash Photolysis Spectrometer (Applied Photophysics, UK). Samples were excited with the frequency tripled light from the Spotlight Compact 100 (InnoLas, Germany) Nd:YAG laser at 355 nm (pulse duration: 8 ns, energy: 10 mJ/pulse). The concentration of the BAPOs in acetonitrile solution was adjusted to achieve an absorbance of approximately 0.3 at 355 nm. The transient absorption spectra were recorded in a quartz cuvette (1 cm x 1 cm) using a flow system driven by a peristaltic pump (0.012 L/min).

**Femtosecond Pump Probe Spectroscopy.** UV-Vis steady state absorption spectra of BAPO (**1**) and BAPO-OH (**2**) were measured with a Varian Cary 500 spectrometer in a 1 mm quartz glass cuvette (SUPRASIL; Hellma) and methylisobutyrate (MIB) as solvent in a spectral region from 200 to 800 nm at ambient temperature. Femtosecond pump-probe experiments were performed with a commercial femtosecond laser system (2210, Clark-MXR) consisting of a diode pumped erbium-doped fibre oscillator and a regenerative Ti:sapphire amplifier (RGA) pumped by a Nd:YAG laser. After optical compressing, pulses at a central wavelength of 775 nm with a pulse duration of about 160 fs were generated at a typical energy of 1.55 mJ per pulse and a repetition rate of 1 kHz. The detailed experimental setup and description of the time-resolved pump-probe experiment are reported in the literature.<sup>S3</sup> Briefly, the output of the femtosecond laser pumped two non-collinear optical parametric amplifier systems (NOPA, Clark-MXR), one for probe pulse tuning within 470 and 750 nm. The second NOPA and the temporally stretched laser fundamental (some tens  $\mu$ J) were used for sum-frequency mixing in

order to generate tunable pump pulses in the UV region. The pump pulses as well as the probe pulses were temporally compressed by the help of prism compressors to 100-150 fs depending on wavelengths. Experiments were performed by temporally delaying the probe pulse beam by a computer-controlled translation stage (Physik Instrumente) relative to the pump pulses. Both beams were focused into a 1 mm absorption cuvette (stirred by a micro fish) under magic angle ( $54.7^\circ$ ) conditions to avoid anisotropic effects and adjusted for temporal and spatial overlap in the sample. Using Si photodiodes, the change of the optical density ( $\Delta OD$ ) as function of a variable delay of the probe pulse was recorded with and without excitation by mechanically chopping at 500 Hz.

**Time-Resolved Electron Paramagnetic Resonance Spectroscopy (TR EPR).** Time-resolved EPR spectra were taken on a Bruker ESP 300E X-band spectrometer (without field modulation, static magnetic field) equipped with a LeCroy 9400 dual 125 MHz digital oscilloscope and using a frequency tripled Brilliant B Nd:YAG laser (Quantel, France, 20 Hz repetition rate, 355 nm, ca. 10 mJ/pulse, ca. 8 ns). The system is controlled using the fsc2 software developed, kindly provided and maintained by Dr. J. T. Toerring (Berlin). Approximately 10 mM argon saturated  $\text{CH}_3\text{CN}$  sample solutions were pumped through a quartz flat cell (ca. 2-3 mL/min) in the rectangular cavity of the EPR spectrometer at room temperature.

**Pulsed Laser Polymerization (PLP).** PLP samples were prepared with a concentration of  $c_{\text{Photoinitiator}} = 5 \cdot 10^{-3} \text{ mol} \cdot \text{L}^{-1}$  in methyl methacrylate or butyl acrylate/acetonitrile (sample volume  $\sim 0.5$  mL) and freed from oxygen by purging with nitrogen for 2 minutes. Subsequently the samples were individually placed into the sample holder, which was held at a constant temperature of  $0^\circ \text{C}$  by a thermostat (model: 1196D, VWR, Darmstadt, Germany). Polymerizations were carried out by an excimer laser system (Coherent XS-500, XeF,  $\lambda = 351$  nm, frequency variable from 1-500 Hz) at a laser energy of 0.35 mJ/pulse (custom-build metal filter was implemented to reduce the laser energy) at a frequency of 100 Hz with 90,000 pulses. After the polymerization, the remaining monomer was evaporated.

**Surfactant Free Emulsion Polymerization (SFEP).** 11.2 mg of BAPO-OH (2.05 mol% with respect to methyl methacrylate) and 4.7 mg of  $\text{NaHCO}_3$  (1.8 eq. with respect to BAPO-OH) were dissolved in 3.5 mL of deionized water. 0.163 mL of methyl methacrylate (1.53 mmol) and a magnetic stir bar were added and oxygen was removed by bubbling with argon. The emulsion was irradiated for 30 minutes with a Hamamatsu Lightningcure LC4 Hg-Xe lamp ( $3500 \text{ mW} \cdot \text{cm}^{-2}$ ,  $\lambda_{\text{max}} = 365 \text{ nm}$ ).

**Electrospray Ionization Mass Spectrometry (ESI-MS).** ESI-MS spectra were recorded on a Q Exactive (Orbitrap) mass spectrometer (Thermo Fisher Scientific, San Jose, CA, USA) equipped with an HESI II probe. The instrument was calibrated in the  $m/z$  range 74-1822 using premixed calibration solutions (Thermo Scientific). A constant spray voltage of 4.7 kV and a dimensionless sheath gas of 5 were applied. The capillary temperature and the S-lens RF level were set to 320 °C and 62.0, respectively. The samples were dissolved with a concentration of 0.05 mg·mL<sup>-1</sup> in a mixture of THF and MeOH (3:2) containing 100 μmol of sodium triflate and infused with a flow of 5 μL·min<sup>-1</sup>.

**Photolysis for ESI-MS.** BAPO (**1**) and BAPO-OH (**2**) were dissolved in acetonitrile ( $c = 5 \cdot 10^{-3}$  mol·L<sup>-1</sup>, ~0.5 mL) and freed from oxygen by purging with nitrogen for 2 minutes. Photolysis was performed at room temperature at a laser energy of 1.50 mJ/pulse and a frequency of 200 Hz with 10,000 pulses (Coherent XS-500, XeF,  $\lambda = 351$  nm).

**Trapping experiments.** BAPO-OH (**2**) was put in a custom-made EPR tube and anhydrous ethanol was added. It was sealed under argon and irradiated for 90 seconds with a Hamamatsu Lightningcure LC4 Hg-Xe lamp (3500 mW·cm<sup>-2</sup>,  $\lambda_{\max} = 365$  nm). For NMR analysis, the glass tube was put in an NMR tube containing THF-*d*8.

**<sup>1</sup>H Chemically Induced Dynamic Nuclear Polarization spectroscopy (CIDNP) and <sup>31</sup>P Nuclear Magnetic Resonance spectroscopy (NMR).** <sup>1</sup>H and <sup>31</sup>P NMR as well as CIDNP experiments were carried out with a 200 MHz Bruker AVANCE DPX spectrometer equipped by a custom-made CIDNP probe head. A Quantel Nd:YAG Brilliant B (355 nm, ~60 mJ/pulse, pulse length ~8–10 ns) operating at 20 Hz served as light source. The typical <sup>1</sup>H CIDNP timing sequence consists of the following parts: composite pulse presaturation, laser flash, 90° radiofrequency detection pulse, and FID. “Dummy” CIDNP spectra without the application of a light pulse were recorded to ensure an effective suppression of the parent NMR spectra. Chemical shifts of the <sup>1</sup>H NMR experiments ( $\delta_{\text{H}}$ ) are reported in ppm relative to tetramethylsilane (TMS) using the residual deuterated solvent signals as an internal reference (CD<sub>3</sub>CN,  $\delta_{\text{H}} = 1.94$  ppm). Chemical shifts of the <sup>31</sup>P NMR experiments ( $\delta_{\text{P}}$ ) are reported in ppm relative to phosphoric acid solution (85 % in D<sub>2</sub>O).

**UV-Vis Spectroscopy.** UV-Vis spectra were recorded on a Shimadzu UV-3101PC UV-Vis-NIR scanning spectrophotometer in THF ( $c = 1$  mM).

**Computational Methods.** The geometries of **1** and **2** in its S<sub>0</sub> ground state and T<sub>1</sub> triplet state and the geometries of radicals **P1** and **P2** in its D<sub>0</sub> doublet and Q<sub>1</sub> quartet state have been optimized by B3LYP/def2-TZVP method.<sup>S4-S7</sup> The vertical excitations S<sub>0</sub>-S<sub>1</sub>, T<sub>1</sub>-T<sub>n</sub>, D<sub>0</sub>-D<sub>n</sub> and

$Q_1$ - $Q_n$  have been computed by TD-CAM-B3LYP/TZVP method<sup>S8,S9</sup> accounting for long-range effects for an appropriate description of  $n\pi^*$  and charge-transfer states. A benchmark of the  $D_0$ - $D_1$  transition in radical **P2** by CASSCF(11,9)/NEVPT2 method resulted in 444 nm compared to 477 nm by CAM-B3LYP for the  $D_1$   $n\pi^*$  transition indicating an underestimation of the  $n\pi^*$  radical transition by about 0.2 eV. This is in contrast to the  $\sim$ 0.2 eV overestimation of the  $n\pi^*$  transition by CAM-B3LYP of the neutral compounds as compared to experiments (Fig. S2). The cleavage of radical **P2** was investigated by computation of the bond dissociation energy ( $BDE = E[\mathbf{MP}] + E[\mathbf{M}'] - E[\mathbf{P2}]$ ) and by calculation of the C-P bond dissociation curve. The UHF-LPNO-CEPA/2 method<sup>S10</sup> is recommended for reaction energies<sup>S11</sup> using quasirestricted orbitals (QRO). It was described to give similar BDEs compared to the CCSD(T) method for  $\alpha$ -hydroxyalkyl hydroperoxide decomposition.<sup>S12</sup> Although bond cleavage of a radical is a multireference problem, UHF-LPNO-CEPA/2 can give the upper limit of BDE and dissociation barrier. Therefore, UHF-LPNO-CEPA/2 and, for comparison, UB3LYP were applied with the TZVP basis set for these calculations. The bond dissociation curves were computed by fixing the C-P distances on geometries optimized by the UB3LYP/6-311+G\*\* method. The gas phase energies for BDE and the bond dissociation barrier were recalculated in acetonitrile by applying the conductor-like screening model (COSMO).<sup>S13</sup> All computations were performed with the program *ORCA*.<sup>S11</sup> Orbitals were depicted with *gabedit*<sup>S14</sup> applying contour values of 0.05 au.

## 2 TR EPR

The TR EPR spectrum of **2** is depicted in Fig. S1. The signal of mesityl radical **M** is in the center at  $g = 2.0005(1)$ . The EPR pattern of phosphinoyl radical **P2** ( $g = 2.0040(2)$ ;  $A^P = 34.9$  mT) shows enhanced absorption/emission according to the radical-pair mechanism.

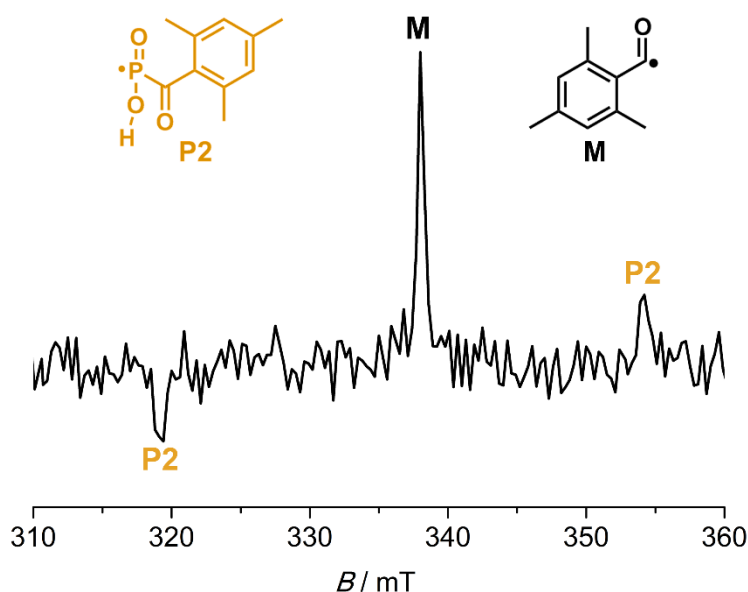


**Fig. S1** TR EPR spectrum of BAPO-OH (**2**) in acetonitrile, integrated signal intensity observed 50-200 ns after the laser pulse ( $\lambda = 355$  nm,  $\sim 10$  mJ/pulse).

## 3 Calculations

**Geometries.** Geometry optimizations in gas phase show that the *cis*-conformation of **1** and **2** is more stable than the *trans*-conformation by 13.5 kJ/mol and 14.3 kJ/mol, respectively. In COSMO (acetonitrile) solvent model the relative stability is confirmed, and therefore, the calculations refer to *cis*-conformations of **1** and **2** with the C=O group *cis* to P-Ph and P-OH, respectively.

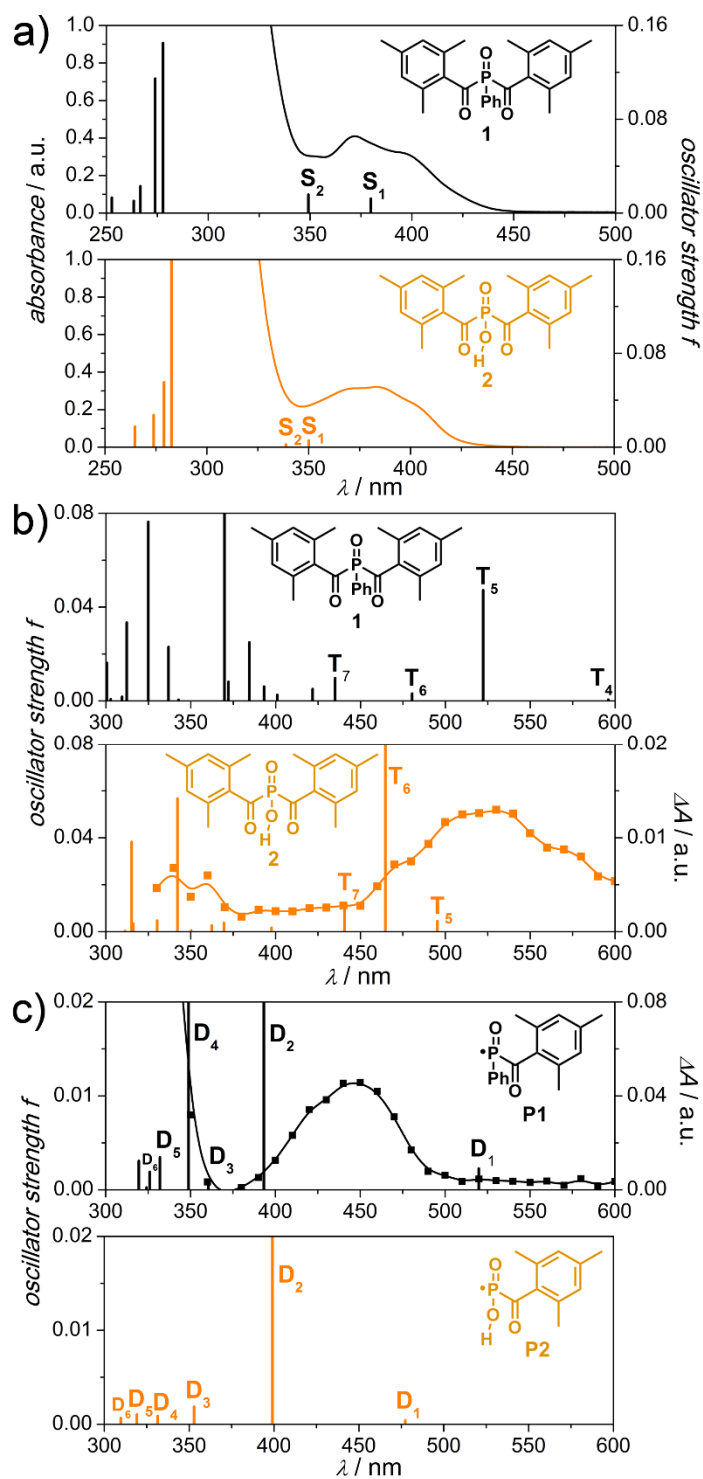
**Absorption spectra.** The singlet  $S_0$ - $S_n$  absorption spectra and the triplet-triplet  $T_1$ - $T_n$  absorption spectra for **1** and **2**, as well as the absorption  $D_0$ - $D_n$  of radicals **P1** and **P2** are displayed in Fig. S2. For both molecules, the first two singlet states  $S_1$  and  $S_2$  are identified as  $n\pi^*$  transitions, while  $S_3$  is a  $\pi\pi^*$  transition. The optimized triplet  $T_1$  state is a  $\pi\pi^*$  transition

for both derivatives. According to El-Sayed's rule,<sup>S17</sup>  $n\pi^*$  states can undergo fast intersystem crossing into  $\pi\pi^*$  triplet states. The computed spectra correlate well with the experimental spectra, taking into account a systematic overestimation of the transitions by about 0.15-0.3 eV, which is known for the CAM-B3LYP method.<sup>S18</sup>

**MO interpretation.** The calculated data (wavelength, energy, oscillator strength) is collated in Table S8-S13 and the corresponding molecular orbitals are depicted in Fig. S17-S22. The singlet transitions  $S_1$  and  $S_2$  of derivatives **1** and **2** occur from the oxygen (and phosphorus) lone pairs ( $n$ ) to the carbonyl groups ( $\pi$ ).  $S_1$  and  $S_2$  of **2** are blueshifted compared to **1**, because the two carbonyl orbitals are well separated in contrast to **1**, where the relevant orbitals are linear combinations of both carbonyl groups. The triplet-triplet transition in the LFP spectrum of **2** (Fig. S2b, peak at 530 nm) can be assigned mainly to the  $T_1 \rightarrow T_6$ -transition, *i.e.* a  $\pi\pi^*$  transition from the carbonyl group to oxygen and phosphorus lone pairs. The first absorption  $D_0 \rightarrow D_1$  of radicals **P1** and **P2** is mainly the transition from the P=O to the C=O group.

**ESIPT.** Additionally, during  $S_1$  optimization of the *cis*-conformer of derivative **2** in gas phase, an excited state intramolecular proton transfer (ESIPT) occurs from P-OH to a carbonyl group resulting in a C-OH...P-O conformation with elongated P-C bond to the second carbonyl group. Unfortunately, the  $S_1$  geometry optimization was not completely converged (*nc*), but resulted in a conformation with completed ESIPT in  $S_1$ . The respective triplet energies at the ESIPT transition geometry and the *nc* geometry are lower than the singlet energies. This points to an alternative pathway of P-C bond cleavage of derivative **2** in gas phase. In solution however, this ESIPT presumably plays a minor role.

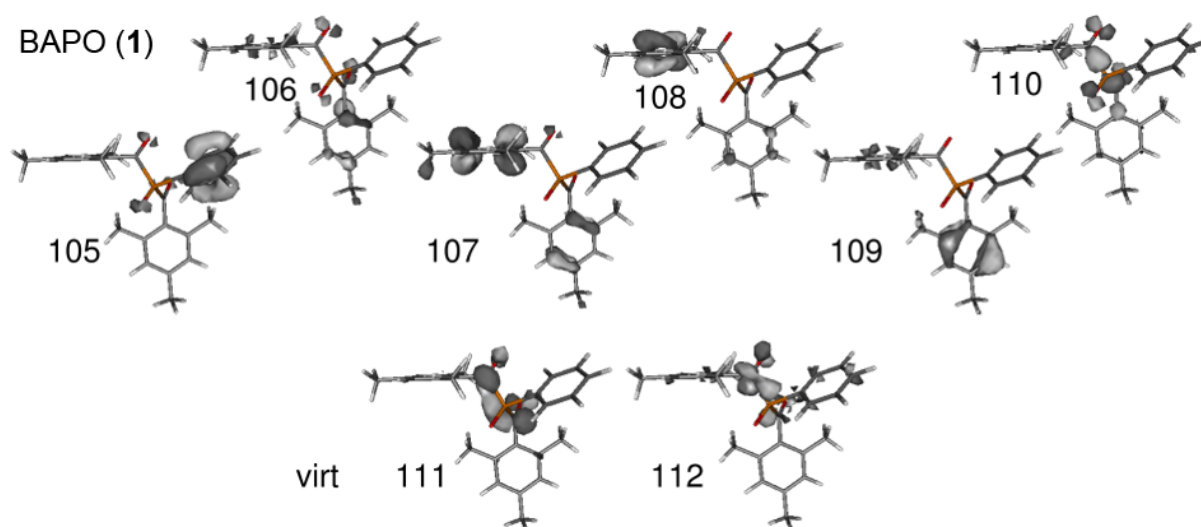




**Fig. S2** a) Experimental and calculated UV-vis absorption spectra of **1** and **2**, b) calculated triplet-triplet transitions for **1** and **2** (including the experimental LFP spectrum of **2**), and c) calculated absorption spectra of **P1** and **P2** (including the experimental LFP spectrum of **P1**). Calculated at the TD-DFT/CAM-B3LYP/TZVP level of theory. Lines are to guide the eye.

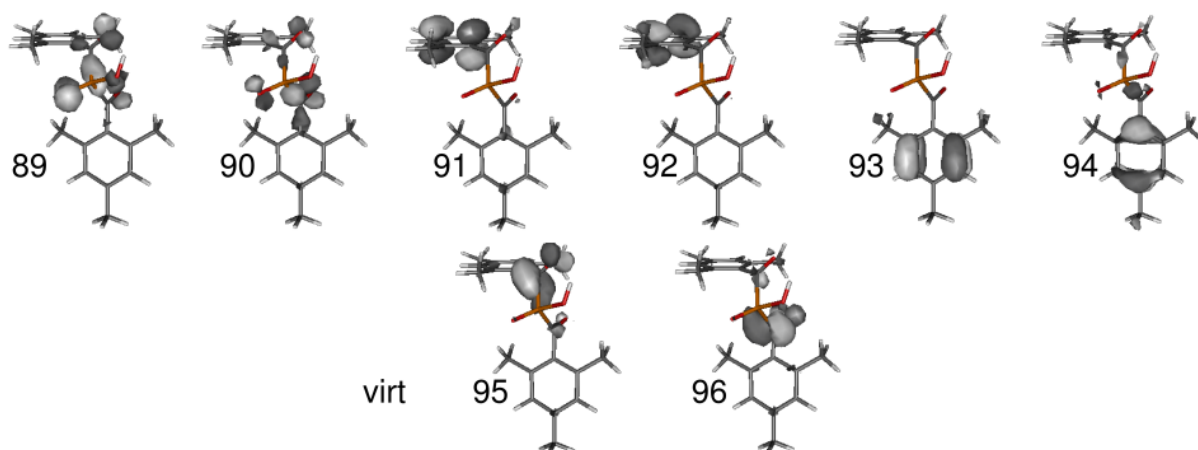
**Table S1** CAM-B3LYP/TZVP Vertical Singlet Excitations of BAPO (1)

BAPO (1)	S <sub>1</sub>	S <sub>2</sub>	S <sub>3</sub>	S <sub>4</sub>	S <sub>5</sub>	S <sub>6</sub>
eV	3.263	3.550	4.463	4.525	4.649	4.707
nm	379.9	349.2	277.8	274.0	266.7	263.4
cm <sup>-1</sup>	26320	28633	35996	36500	37498	37968
f	0.0123	0.0157	0.1450	0.1146	0.0229	0.0104
M01	110 → 111	110 → 112	106 → 111	107 → 111	109 → 111	108 → 111
c	0.53	0.31	0.26	0.33	0.40	0.25
M02	106 → 111	104 → 111	107 → 111	107 → 112	108 → 111	108 → 112
c	0.21	0.19	0.17	0.19	0.25	0.21
M03		106 → 112	110 → 111			109 → 111
c		0.15	0.15			0.16
M04			109 → 111			
c			0.11			

**Fig. S3** Molecular orbitals of BAPO (1) in the S<sub>0</sub> singlet ground state.**Table S2** CAM-B3LYP/TZVP Vertical Singlet Excitations of BAPO-OH (2)

BAPO-OH (2)	S <sub>1</sub>	S <sub>2</sub>	S <sub>3</sub>	S <sub>4</sub>	S <sub>5</sub>	S <sub>6</sub>
eV	3.543	3.660	4.388	4.445	4.527	4.683
nm	350.0	338.8	282.6	279.0	273.9	264.7
cm <sup>-1</sup>	28574	29517	35390	35849	36514	37772
f	0.0055	0.0023	0.1800	0.0553	0.0273	0.0175
M01	90 → 95	90 → 96	91 → 95	91 → 95	92 → 95	93 → 96
c	0.32	0.28	0.45	0.22	0.71	0.58
M02	90 → 96	89 → 95	94 → 96	94 → 96		93 → 95
c	0.21	0.26	0.36	0.21		0.32
M03	89 → 96	90 → 95		94 → 95		
c	0.14	0.13		0.21		
M04	94 → 95			91 → 96		
c	0.12			0.14		

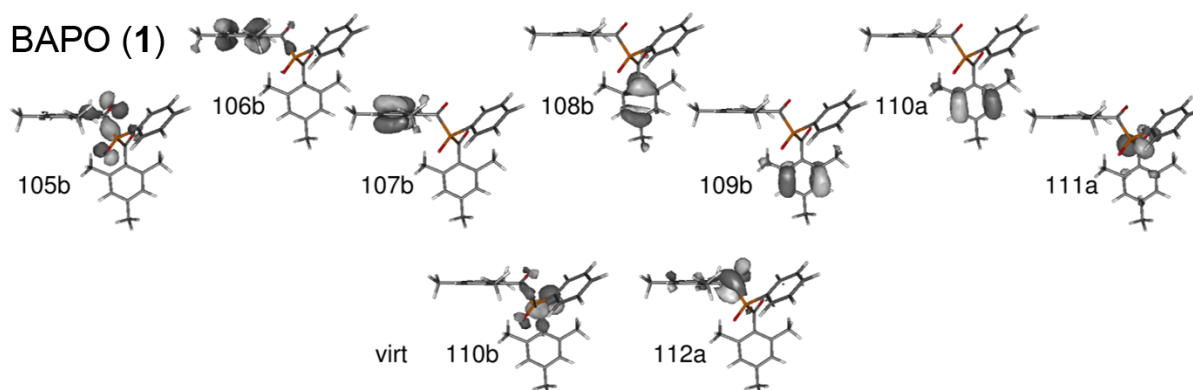
### BAPO-OH (2)



**Fig. S4** Molecular orbitals of BAPO-OH (2) in the  $S_0$  singlet ground state.

**Table S3** CAM-B3LYP/TZVP Triplet Excitations of BAPO (1)

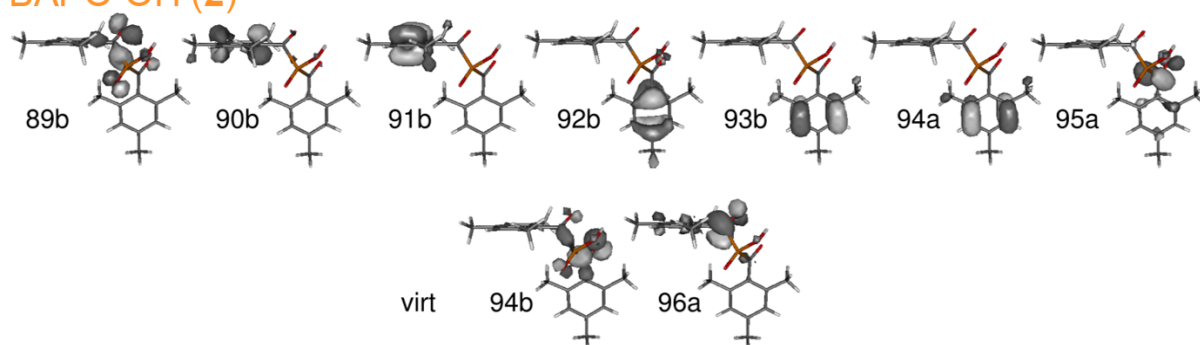
BAPO (1), $T_1 \rightarrow$	$T_2$	$T_3$	$T_4$	$T_5$	$T_6$	$T_7$
<b>eV</b>	1.496	1.804	2.080	2.374	2.581	2.850
<b>nm</b>	828.6	687.3	596.0	522.3	480.4	435.0
<b>cm<sup>-1</sup></b>	12068	14550	16779	19147	20816	22987
<b>f</b>	0.0009	0.0190	0.0005	0.0472	0.0031	0.0097
<b>M01</b>	108b $\rightarrow$ 110b	105b $\rightarrow$ 110b	109b $\rightarrow$ 110b	111a $\rightarrow$ 112a	106b $\rightarrow$ 110b	103b $\rightarrow$ 110b
<b>c</b>	0.80	0.56	0.97	0.74	0.36	0.34
<b>M02</b>		106b $\rightarrow$ 110b			105b $\rightarrow$ 110b	106b $\rightarrow$ 110b
<b>c</b>		0.13			0.23	0.26
<b>M03</b>		111a $\rightarrow$ 112a				
<b>c</b>		0.12				



**Fig. S5** Molecular orbitals of BAPO (1) in the  $T_1$  triplet state.

**Table S4** CAM-B3LYP/TZVP Triplet Excitations of BAPO-OH (2)

BAPO (1), $T_1 \rightarrow$	$T_2$	$T_3$	$T_4$	$T_5$	$T_6$	$T_7$
eV	1.407	1.774	1.980	2.503	2.668	2.814
nm	881.1	699.1	626.2	495.4	464.7	440.6
$\text{cm}^{-1}$	11349	14305	15968	20186	21518	22699
f	0.0022	0.0028	0.0003	0.0045	0.2504	0.0104
M01	92b $\rightarrow$ 94b	89b $\rightarrow$ 94b	93b $\rightarrow$ 94b	90b $\rightarrow$ 94b	95a $\rightarrow$ 96a	91b $\rightarrow$ 94b
c	0.87	0.46	0.99	0.73	0.49	0.96
M02		95a $\rightarrow$ 96a			89b $\rightarrow$ 94b	
c		0.37			0.37	

**BAPO-OH (2)****Fig. S6** Molecular orbitals of BAPO-OH (2) in the  $T_1$  triplet state.**Table S5** CAM-B3LYP/TZVP Doublet Excitations of Phosphinoyl Radical **P1**

P1, $D_0 \rightarrow$	$D_1$	$D_2$	$D_3$	$D_4$	$D_5$	$D_6$
eV	2.385	3.153	3.439	3.553	3.735	3.805
nm	519.9	393.2	360.6	348.9	332	325.9
$\text{cm}^{-1}$	19234	25432	27732	28662	30120	30684
f	0.0023	0.0372	0.0010	0.0261	0.0035	0.0019
M01	68b $\rightarrow$ 71b	71a $\rightarrow$ 72a	69b $\rightarrow$ 71b	66b $\rightarrow$ 71b	65b $\rightarrow$ 71b	70b $\rightarrow$ 71b
c	0.74	0.65	0.39	0.59	0.37	0.52
M02			70b $\rightarrow$ 71b		68b $\rightarrow$ 72b	
c			0.28		0.19	

### Radical P1

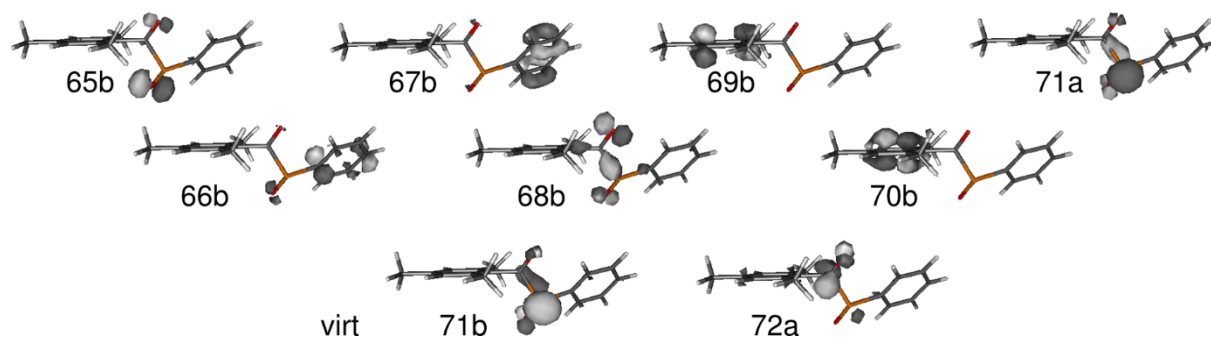


**Fig. S7** Molecular orbitals of radical **P1** in the  $D_0$  doublet state.

**Table S6** CAM-B3LYP/TZVP Doublet Excitations of Phosphinoyl Radical **P2**

<b>P<sub>2</sub>, D<sub>0</sub>→</b>	<b>D<sub>1</sub></b>	<b>D<sub>2</sub></b>	<b>D<sub>3</sub></b>	<b>D<sub>4</sub></b>	<b>D<sub>5</sub></b>	<b>D<sub>6</sub></b>
<b>eV</b>	2.597	3.106	3.513	3.741	3.884	4.004
<b>nm</b>	477.3	399.1	352.9	331.4	319.2	309.7
<b>cm<sup>-1</sup></b>	20951	25056	28337	30175	31328	32289
<b>f</b>	0.0004	0.0333	0.0019	0.0009	0.0010	0.0006
<b>M01</b>	55a → 56a	52b → 55b	53b → 55b	53a → 56a	54b → 55b	50b → 55b
<b>c</b>	0.56	0.58	0.46	0.30	0.60	0.40
<b>M02</b>	52b → 55b	55a → 56a	54b → 55b	53b → 55b	53b → 55b	52b → 56b
<b>c</b>	0.29	0.27	0.23	0.14	0.29	0.35
<b>M03</b>				53b→56b		
<b>c</b>				0.11		

### Radical P2

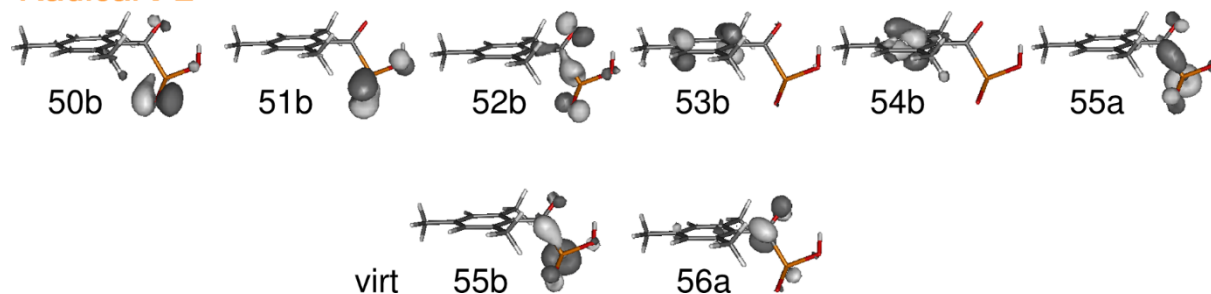


**Fig. S8** Molecular orbitals of radical **P2** in the  $D_0$  doublet state.

**Radical dissociation.** The *cis*-conformation of **P2** is thermodynamically more stable than the *trans*-conformer (Fig. S9, 1 and 2), furthermore, a significantly lower bond dissociation energy (BDE) was calculated (UHF-LPNO-CEPA/2 method: ca. 44 kJ/mol for *cis* compared to 75 kJ/mol for *trans*). Therefore, we can conclude that the bond cleavage of **P2** occurs from the *cis*-conformer.

The experimentally proposed bond cleavage of radical **P2** is presented in Fig. S9 as computed by the UB3LYP/6-311++G\*\* method. Cleavage of the *cis*-conformer occurs in two steps. The first step is homolytic cleavage of the C(O)-P(O) bond, which is accompanied by the formation of a hydrogen bond between the hydroxy-H and the adjacent carbonyl-O of **MP** and **M'**, respectively. In the second step the hydrogen bond is broken.

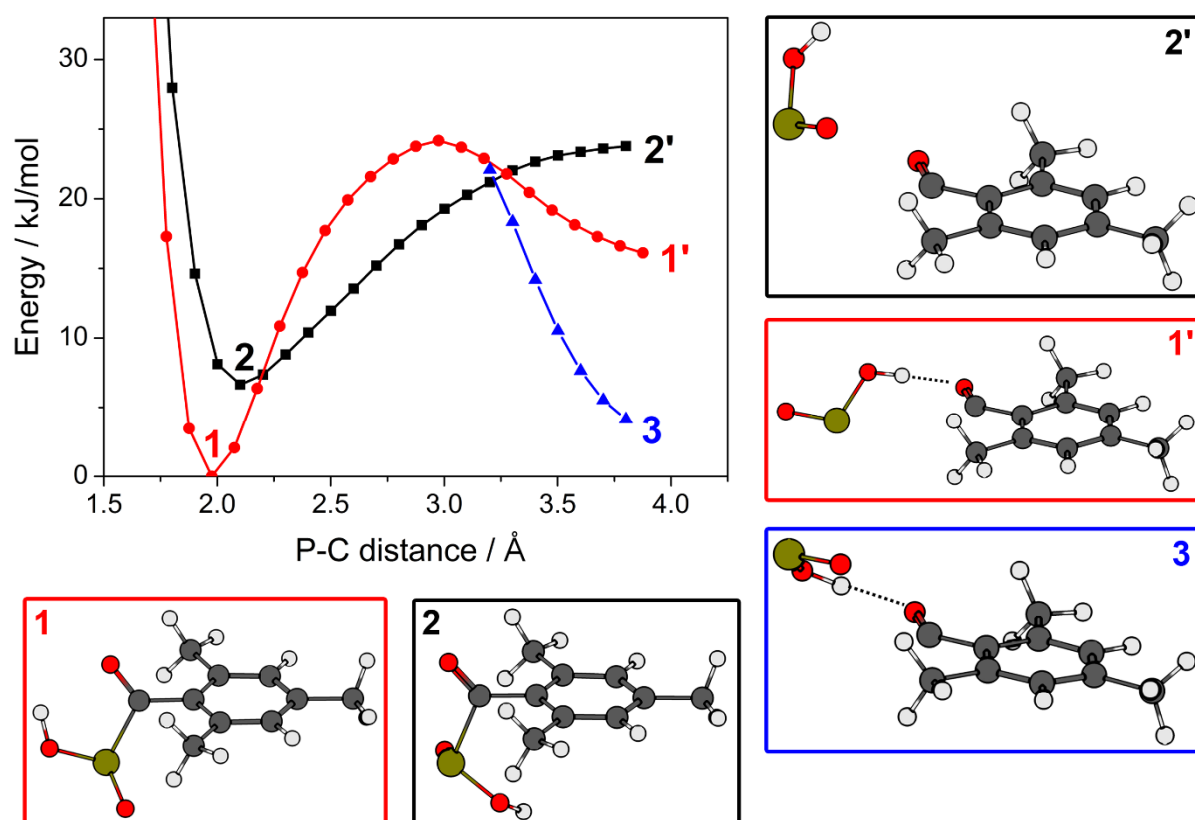


**Fig. S9** DFT (UB3LYP/6-311++G\*\*) calculated reaction pathways of the C-P bond cleavage of radical **P2** from different starting conformations (1, *cis*, red curve and 2, *trans*, black curve). Cleavage and rearrangement of the *cis*-conformer, results in a hydrogen-bonded adduct of radical **M'** and **MP** (conformations 1', red curve and 3, blue curve, respectively). The less stable *trans*-conformation dissociates by forming separated molecules **M'** and **MP** at 3.8 Å (black curve).

Table S7 compares the energies of the C-P bond cleavage of radical **P2** (*cis*-conformer 1, Fig. S9) in gas phase and in acetonitrile, calculated with different methods (UB3LYP and UHF-LPNO-CEPA/2). The calculated BDE of 44 kJ/mol (in acetonitrile) is the overall reaction energy for both steps (rearrangement and breaking of the hydrogen bond). A relative energy of

32 kJ/mol (in acetonitrile) was calculated for the rearranged geometry (1', Fig. S9). The difference between the two energies is 12 kJ/mol which is in the range of a hydrogen bond in acetonitrile.

**Table S7** BDEs of **P2** (*cis*-conformer 1) and Relative Energies of Points of the Bond Cleavage Curves (Fig. S9, red curve) with Different Methods

<b>P2 (<i>cis</i>-conformer 1)</b>	<b>UB3LYP/def2-TZVP</b>		<b>UHF-LPNO-CEPA/2</b>	
	gas	MeCN	gas	MeCN
<b>BDE / kJ/mol</b>	35.0	22.6	56.1	43.7
<b>Barrier (2.8 Å)<sup>a</sup> / kJ/mol</b>	28.3	22.7	50.0	38.9
<b>Rearranged Geometry (1' at 3.8 Å)<sup>a</sup> / kJ/mol</b>	17.9	14.6	39.3	32.5

<sup>a</sup> single point energies at UB3LYP/6-311++G\*\* geometries

## 4 Polymerization Experiments

### 4.1 PLP-ESI-MS of methyl methacrylate initiated by BAPO (1) and BAPO-OH (2) under bulk conditions

The following nomenclature was adopted to label the observed ESI-MS polymer signals. Disproportionation and combination products are distinguished by superscripts D and C, respectively. Disproportionation peaks occur in pairs with a mass difference of 2 amu. These peaks are labeled **XH** or **X=**, where **X** defines the photoinitiator derived end groups of the polymer chain in  $\alpha$ -position: **M** for the mesitoyl moiety, and **P#** for the phosphinoyl moiety. The end group in  $\omega$ -position of the polymer chain is denoted as = (bearing a double bond) or **H** (bearing no double bond), depending on the role of the reactive site during the H-abstraction of the disproportionation process, or as **X** for combination products. Polymer species denoted with **T#** result from BAPOs which initiated twice (cleavage of both mesitoyl groups).

Fig. S10a depicts the ESI-MS overview spectrum of poly(methyl methacrylate) (pMMA) synthesized via PLP ( $\lambda = 351$  nm, 0.35 mJ/pulse, 100 Hz) under bulk conditions ( $c_{\text{photoinitiator}} = 5 \cdot 10^{-3}$  mol·L<sup>-1</sup>) photoinitiated by **1**. A zoom into one repeating unit of the polymer is displayed in Fig. S10b and a complete assignment of the signals is listed in Table S8. Scheme S1 depicts the structures of the assigned disproportionation and combination products. Methyl

methacrylate initiated by **1** results in the formation of the expected polymer chains end-capped with mesitoyl ( $M^D$ ,  $MH^D$ ,  $MM^C$ ) and P-containing groups ( $P1^D$ ,  $P1H^D$ ,  $T1^D$ ,  $T1H^D$ ,  $T1H^D$ ,  $P1M^C$ ).

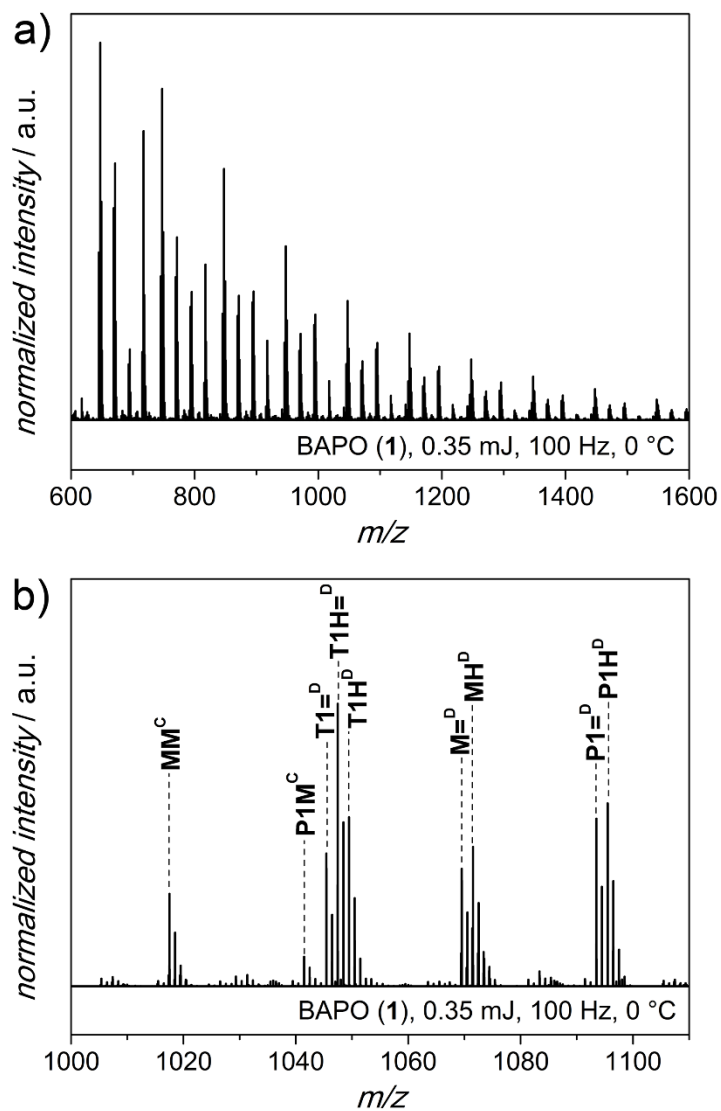
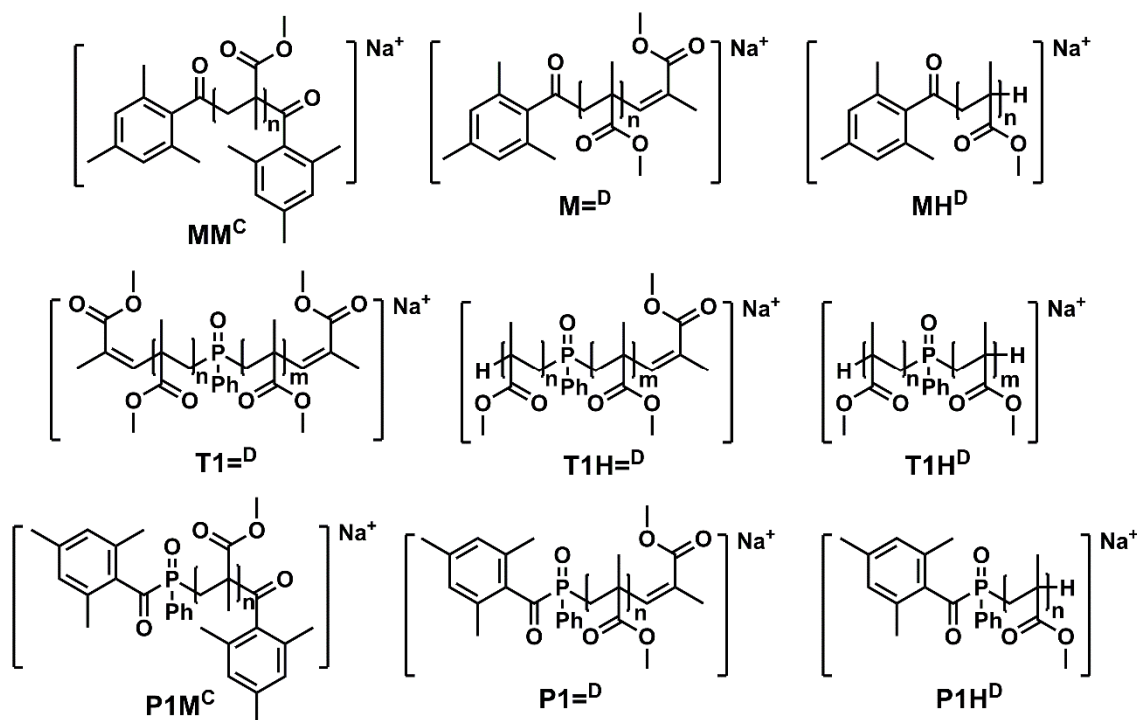


**Fig. S10** a) ESI-MS spectrum of poly(methyl methacrylate) synthesized via PLP ( $\lambda = 351$  nm, 0.35 mJ/pulse, 100 Hz, 90,000 pulses) initiated by BAPO (**1**) and b) zoom into one repeating unit.





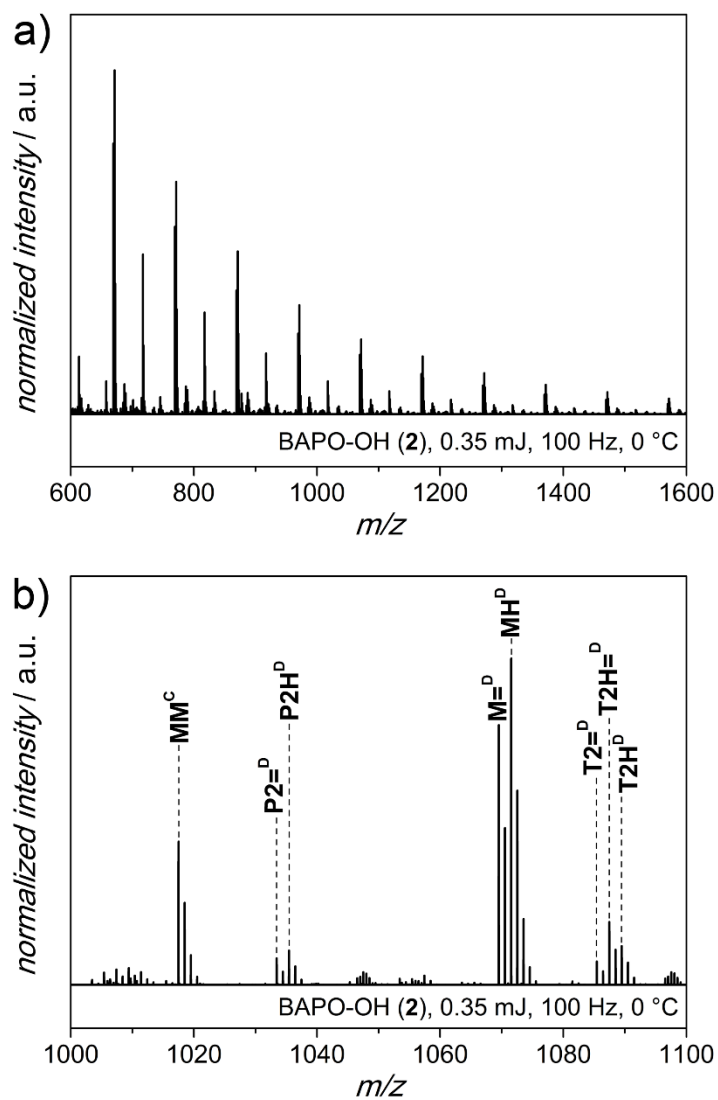
**Scheme S1** Disproportionation and Combination Products of the PLP ( $\lambda = 351$  nm, 0.35 mJ/pulse) of Poly(Methyl Methacrylate) Initiated by BAPO (**1**), as Detected by ESI-MS.

**Table S8** Overview of the Assigned Signals of Poly(Methyl Methacrylate) Synthesized via PLP ( $\lambda = 351$  nm, 0.35 mJ/pulse) Initiated by BAPO (**1**), as Detected by ESI-MS

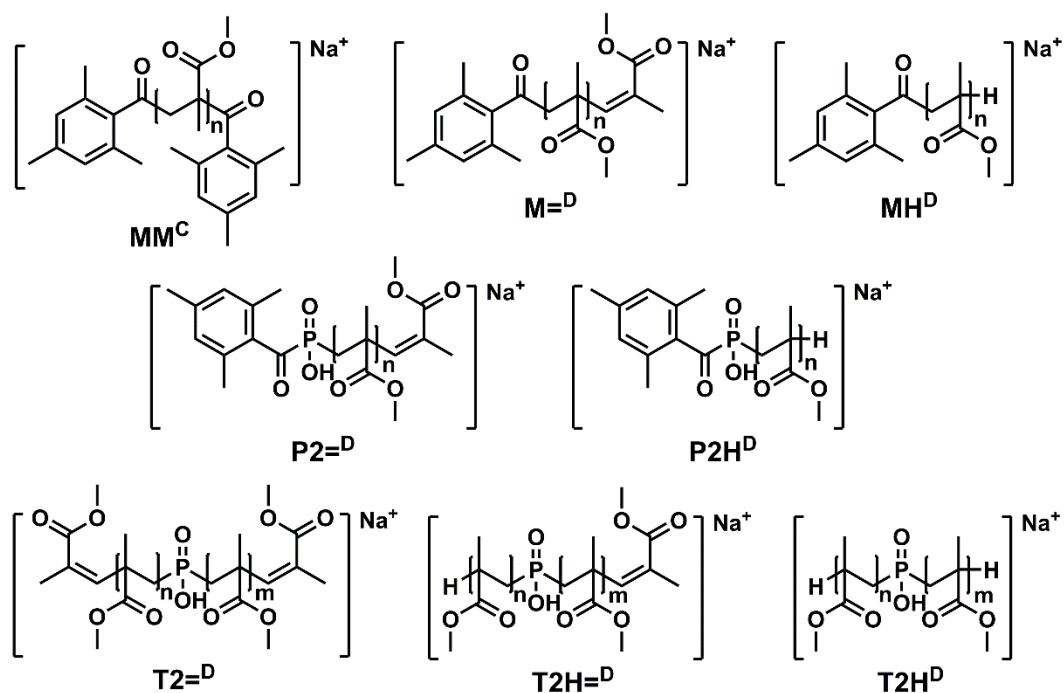
Species	$(m/z)^{\text{exp}}$	$(m/z)^{\text{theo}}$	$\Delta(m/z)$
<b>MM<sup>C</sup></b>	1017.5175	1017.5188	0.0013
<b>P1M<sup>C</sup></b>	1041.4728	1041.4742	0.0014
<b>T1=D</b>	1045.4523	1045.4538	0.0015
<b>T1H=D</b>	1047.4681	1047.4695	0.0014
<b>T1H<sup>D</sup></b>	1049.4832	1049.4851	0.0019
<b>M=D</b>	1069.5335	1069.5348	0.0013
<b>MH<sup>D</sup></b>	1071.5494	1071.5505	0.0011
<b>P1=D</b>	1093.4892	1093.4902	0.0010
<b>P1H<sup>D</sup></b>	1095.5044	1095.5059	0.0015

Fig. S11a depicts the ESI-MS overview spectrum of pMMA synthesized via PLP under bulk conditions photoinitiated by **2**. A zoom into one repeating unit of the polymer is displayed in Fig. S11b and a complete assignment of the signals is listed in Table S9. Scheme S2 depicts the structures of the assigned disproportionation and combination products. Methyl methacrylate initiated by **2** likewise results in the formation of polymer chains end-capped with mesityl (**M=D**, **MH<sup>D</sup>**, **MM<sup>C</sup>**) and P-containing groups (**P2=D**, **P2H<sup>D</sup>**, **T2=D**, **T2H=D**, **T2H<sup>D</sup>**). It can be

concluded that the short-lived phosphinoyl radicals **P2** are readily quenched by the monomer under bulk conditions.



**Fig. S11** a) ESI-MS spectrum of poly(methyl methacrylate) synthesized via PLP ( $\lambda = 351$  nm, 0.35 mJ/pulse, 100 Hz, 90,000 pulses) initiated by BAPO-OH (**2**) and b) zoom into one repeating unit.



**Scheme S2** Disproportionation and Combination Products of the PLP ( $\lambda = 351$  nm, 0.35 mJ/pulse) of Poly(Methyl Methacrylate) Initiated by BAPO-OH (**2**), as Detected by ESI-MS.

**Table S9** Overview of the Assigned Signals of Poly(Methyl Methacrylate) Synthesized via PLP ( $\lambda = 351$  nm, 0.35 mJ/pulse) Initiated by BAPO-OH (**2**), as Detected by ESI-MS

Species	$(m/z)^{\text{exp}}$	$(m/z)^{\text{theo}}$	$\Delta(m/z)$
<b>MM<sup>C</sup></b>	1017.5201	1017.5188	0.0013
<b>P2=<sup>D</sup></b>	1033.4551	1033.4538	0.0013
<b>P2H<sup>D</sup></b>	1035.4709	1035.4695	0.0014
<b>M=<sup>D</sup></b>	1069.5364	1069.5348	0.0016
<b>MH<sup>D</sup></b>	1071.5520	1071.5505	0.0015
<b>T2=<sup>D</sup></b>	1085.4714	1085.4699	0.0015
<b>T2H=<sup>D</sup></b>	1087.4872	1087.4855	0.0017
<b>T2H<sup>D</sup></b>	1089.5025	1089.5012	0.0013

## 4.2 PLP-ESI-MS of butyl acrylate (0.5 M in acetonitrile) initiated by BAPO (1) and BAPO-OH (2)

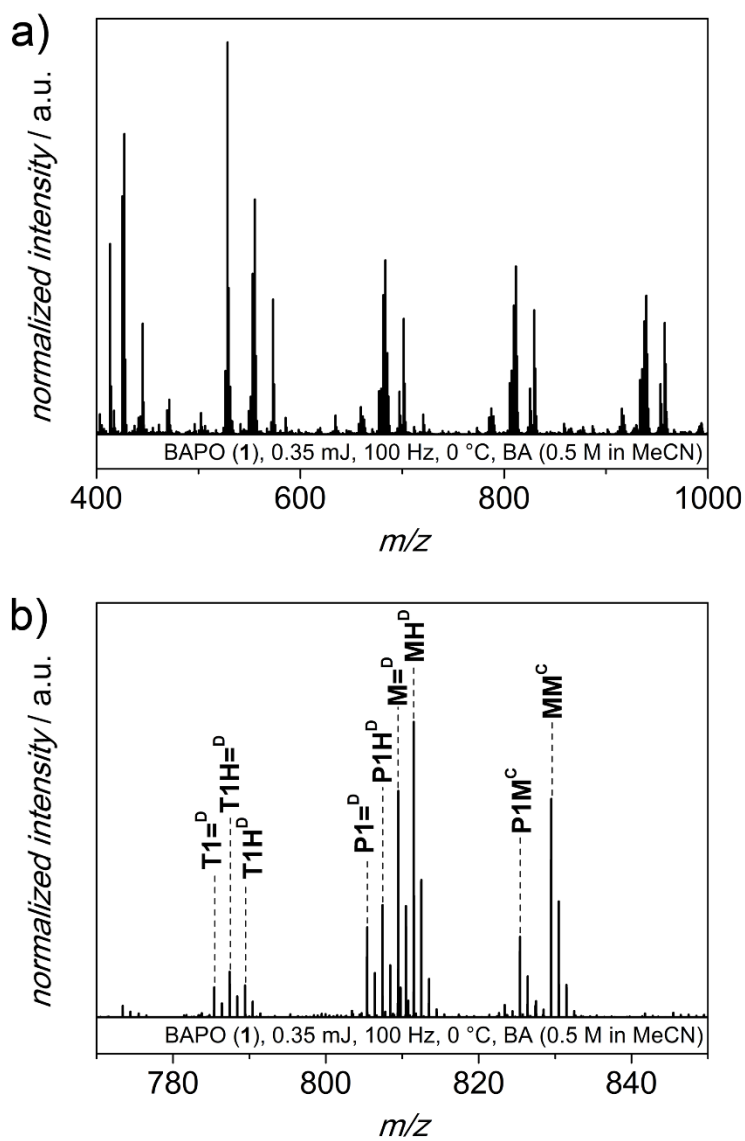
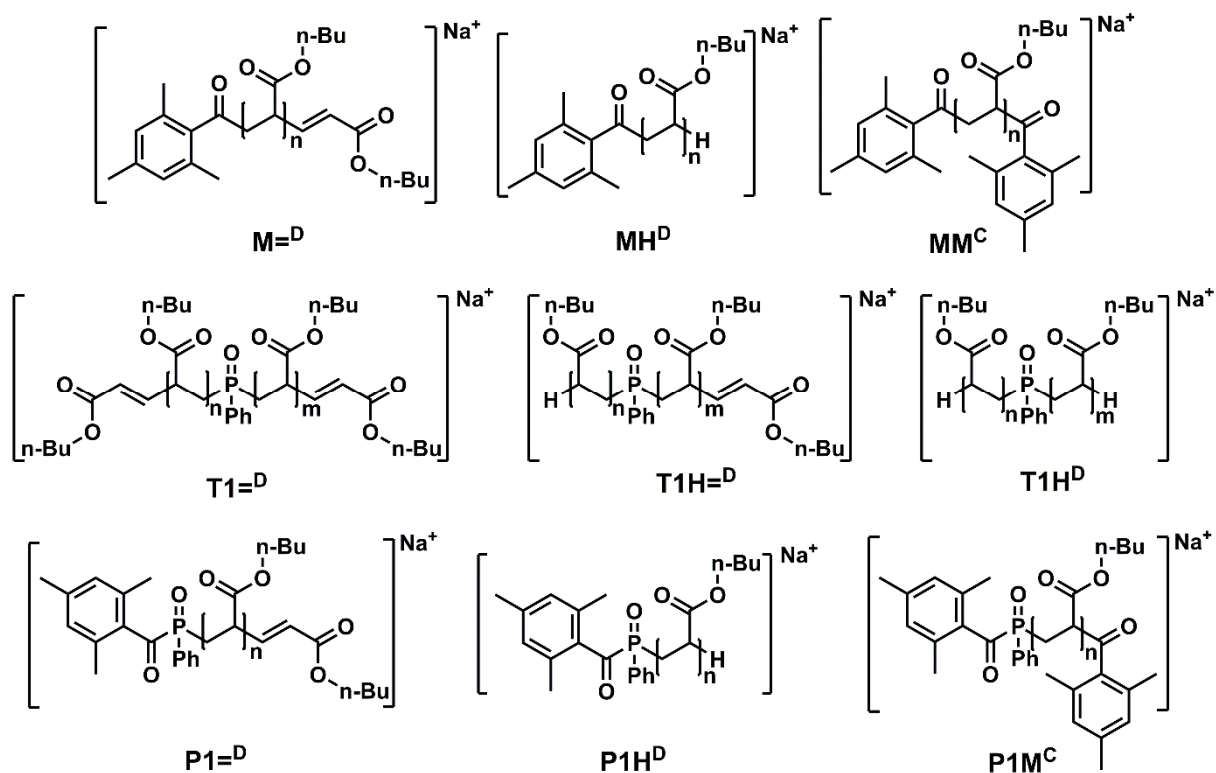


**Fig. S12** a) ESI-MS spectrum of poly(butyl acrylate) synthesized via PLP ( $\lambda = 351$  nm, 0.35 mJ/pulse, 100 Hz, 90,000 pulses, 0.5 M butyl acrylate in acetonitrile) initiated by BAPO (1) and b) zoom into one repeating unit.



**Scheme S3** Disproportionation and Combination Products of the PLP ( $\lambda = 351$  nm, 0.35 mJ/pulse) of Poly(Butyl Acrylate) Initiated by BAPO (**1**), as Detected by ESI-MS.

**Table S10** Overview of the Assigned Signals of Poly(Butyl Acrylate) Synthesized via PLP ( $\lambda = 351$  nm, 0.35 mJ/pulse, 0.5 M Butyl Acrylate in Acetonitrile) Initiated by BAPO (**1**), as Detected by ESI-MS

Species	$(m/z)^{\text{exp}}$	$(m/z)^{\text{theo}}$	$\Delta(m/z)$
<b>T1=D</b>	785.4010	785.4006	0.0004
<b>T1H=D</b>	787.4168	787.4162	0.0006
<b>T1H<sup>D</sup></b>	789.4325	789.4319	0.0006
<b>P1=D</b>	805.4054	805.4057	0.0003
<b>P1H<sup>D</sup></b>	807.4214	807.4213	0.0001
<b>M=D</b>	809.4817	809.4816	0.0001
<b>MH<sup>D</sup></b>	811.4978	811.4973	0.0005
<b>P1M<sup>C</sup></b>	825.4105	825.4108	0.0003
<b>MM<sup>C</sup></b>	829.4853	829.4867	0.0014

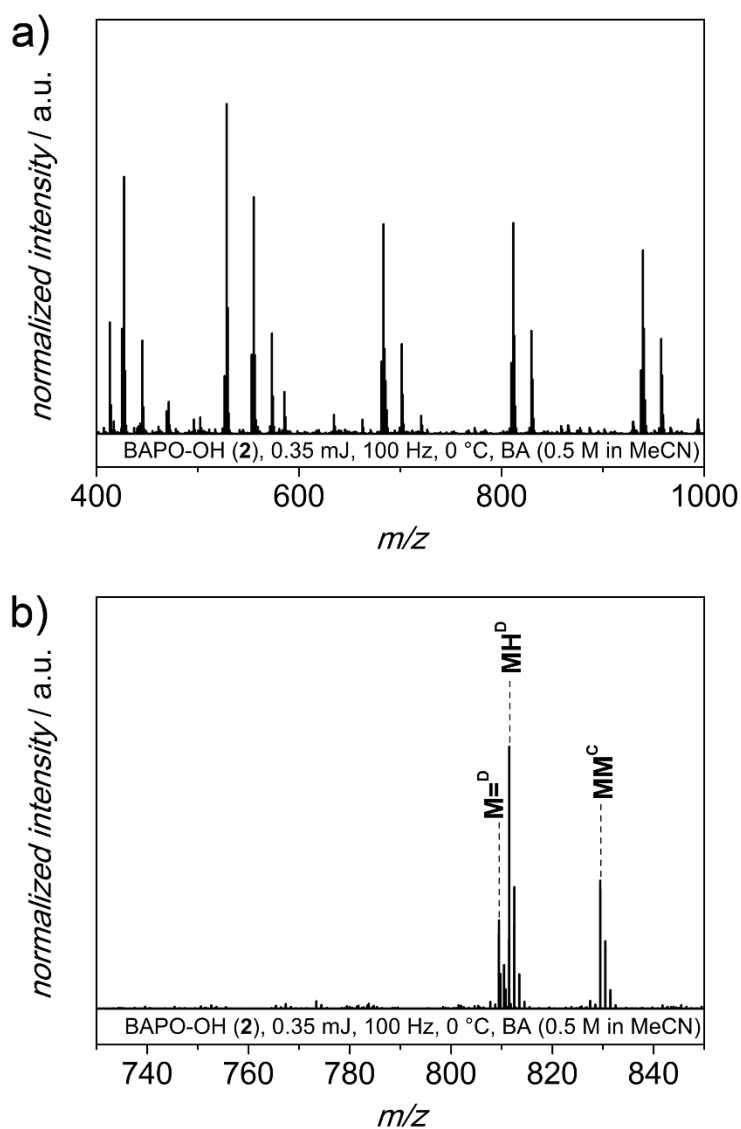


**Fig. S13** a) ESI-MS spectrum of poly(butyl acrylate) synthesized via PLP ( $\lambda = 351$  nm, 0.35 mJ/pulse, 100 Hz, 90,000 pulses, 0.5 M butyl acrylate in acetonitrile) initiated by BAPO-OH (2) and b) zoom into one repeating unit.

**Table S11** Overview of the Assigned Signals of Poly(Butyl Acrylate) Synthesized via PLP ( $\lambda = 351$  nm, 0.35 mJ/pulse, 0.5 M Butyl Acrylate in Acetonitrile) Initiated by BAPO-OH (2), as Detected by ESI-MS

Species	$(m/z)^{\text{exp}}$	$(m/z)^{\text{theo}}$	$\Delta(m/z)$
$M=D$	809.4817	809.4816	0.0001
$MH^D$	811.4978	811.4973	0.0005
$MM^C$	829.4853	829.4867	0.0014

### 4.3 $^1\text{H}$ CIDNP of BAPO (1) and BAPO-OH (2) in the presence of butyl acrylate (0.5 M in acetonitrile)

The  $^1\text{H}$  CIDNP spectrum of **1** in the presence of butyl acrylate (0.5 M in acetonitrile- $d_3$ ) shows polarized signals for the addition of P-centered radical **P1** to butyl acrylate at approximately 3 ppm (**P1BA** and **P1BA'**; Fig. S14b). The signals stem from the alkyl protons of butyl acrylate (marked with h, h' and i, respectively). The singlet at  $\delta = 10.5$  ppm can be assigned to 2,4,6-trimethylbenzaldehyde (**Ald**), resulting from disproportionation (hydrogen transfer) reactions.<sup>S15</sup> The poor suppression of NMR signals can be explained by the high concentration of butyl acrylate.

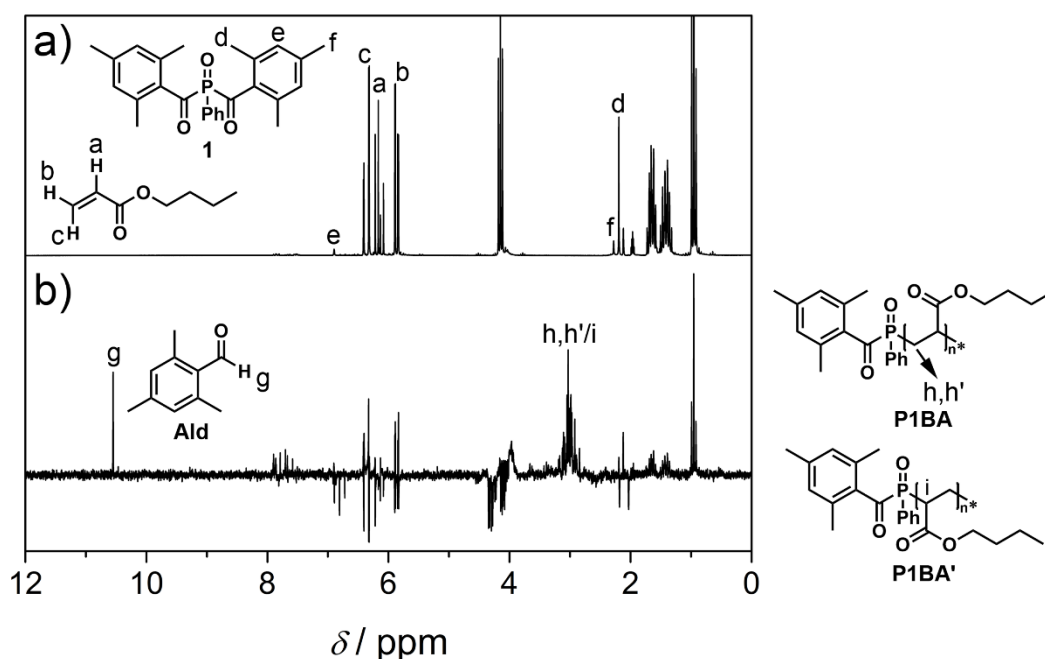


**Fig. S14** a)  $^1\text{H}$  NMR and b)  $^1\text{H}$  CIDNP of BAPO (**1**; 5 mM in acetonitrile- $d_3$ ) in the presence of butyl acrylate (0.5 M).

In contrast,  $^1\text{H}$  CIDNP of **2** in the presence of butyl acrylate only yields products containing mesitoyl radical **M** (Fig. S15b). The singlet at  $\delta = 10.5$  ppm again stems from 2,4,6-trimethylbenzaldehyde (**Ald**). The signals marked with i ( $\delta = 4.45$  to 4.60 ppm) and h, h' ( $\delta = 3.35$  to 3.45 ppm) can be assigned to the alkyl protons of product **MBAM**, resulting from the addition of two mesitoyl radicals **M** to butyl acrylate. No polarized signals indicating the addition of P-centered radical **P2** to butyl acrylate were observed.

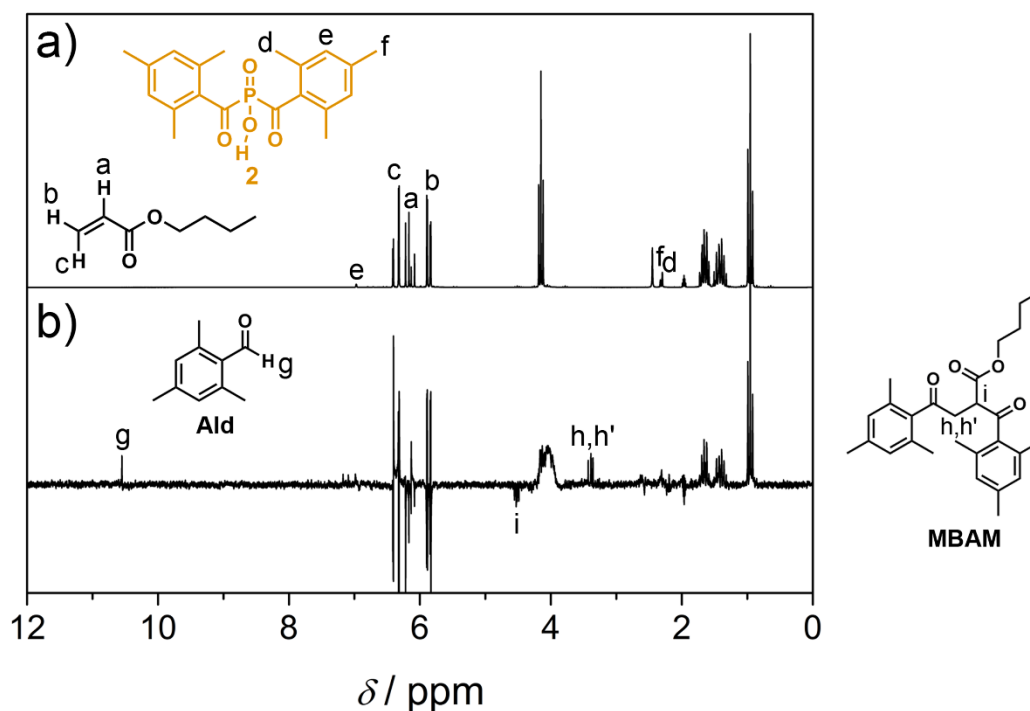


**Fig. S15** a)  $^1\text{H}$  NMR and b)  $^1\text{H}$  CIDNP of BAPO-OH (**2**; 5 mM in acetonitrile- $d_3$ ) in the presence of butyl acrylate (0.5 M).

#### 4.4 Surfactant-free emulsion polymerization (SFEP) of methyl methacrylate initiated by BAPO-ONa (**3**)

BAPO-ONa (**3**) was generated *in situ* by dissolving BAPO-OH (**2**) and 1.8 eq. of  $\text{NaHCO}_3$  in deionized water. Fig. S16a depicts the ESI-MS overview spectrum of pMMA synthesized via SFEP photoinitiated by **3**. A zoom into one repeating unit of the polymer is displayed in Fig. S16b and a complete assignment of the signals is listed in Table S12. Scheme S4 depicts the structures of the assigned disproportionation and combination products. The ESI-MS spectra only show signals of polymer chains end-capped with mesitoyl groups ( $\text{M}=\text{D}$ ,  $\text{MHP}$ ,  $\text{MMC}$ ). No polymeric species with P-containing end groups were detected, pointing to the occurrence of side reactions of phosphinoyl radical **P3**.



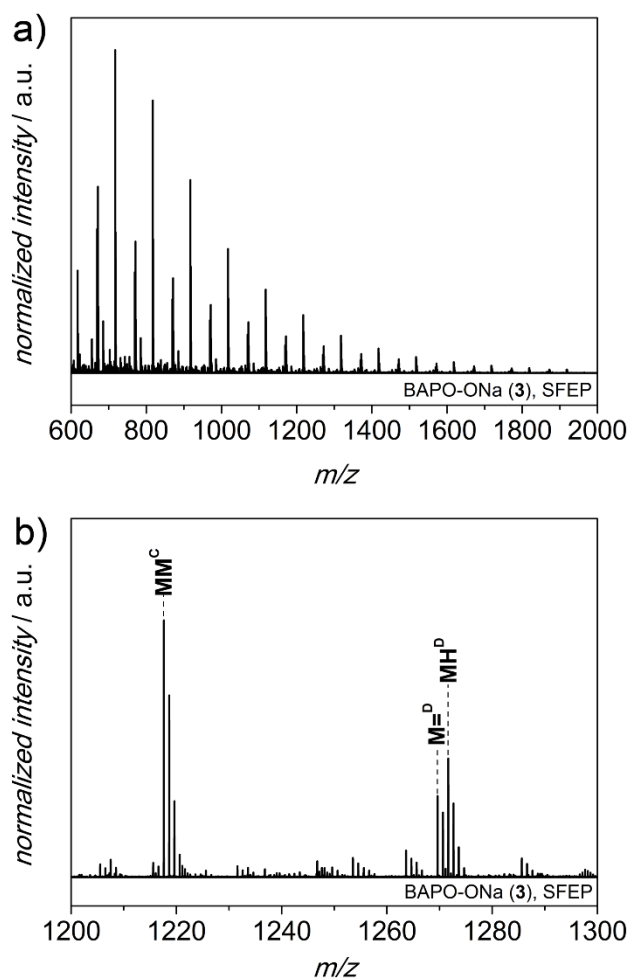
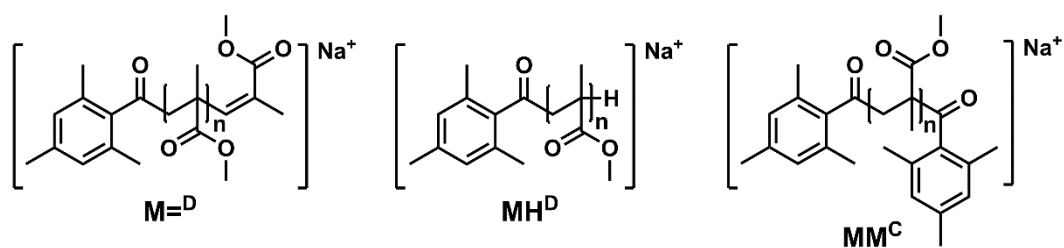


**Fig. S16** a) ESI-MS spectrum of poly(methyl methacrylate) synthesized via SFEP initiated by BAPO-ONa (**3**) and b) zoom into one repeating unit.



**Scheme S4** Disproportionation and Combination Products of the SFEP of Poly(Methyl Methacrylate) Initiated by BAPO-ONa (**3**), as Detected by ESI-MS.

**Table S12** Overview of the Assigned Signals of Poly(Methyl Methacrylate) Synthesized via SFEP Initiated by BAPO-ONa (**3**), as Detected by ESI-MS

Species	$(m/z)^{\text{exp}}$	$(m/z)^{\text{theo}}$	$\Delta(m/z)$
MM <sup>C</sup>	1217.6282	1217.6237	0.0045
M= <sup>D</sup>	1269.6458	1269.6397	0.0061
MH <sup>D</sup>	1271.6600	1271.6553	0.0047

## 5 Photolysis Experiments

### 5.1 <sup>31</sup>P NMR of BAPO-OH (**2**) after photolysis

The <sup>31</sup>P NMR spectra (<sup>1</sup>H decoupled/coupled) of BAPO-OH (**2**) after photolysis (Hg-Xe lamp) are depicted in Fig. S17. The signal at -2.5 ppm stems from residual **2**. The signal of the major product (<sup>31</sup>P  $\delta$  = 5.2 ppm, Fig. S17a) splits to a doublet with <sup>1</sup>J<sub>P-H</sub> of 694 Hz in the <sup>1</sup>H coupled phosphorus spectrum (Fig. S17b). It can be tentatively assigned to phosphonic acid (**PA**; H<sub>3</sub>PO<sub>3</sub>) based on literature data (<sup>31</sup>P  $\delta$  = 1.7-8 ppm, <sup>1</sup>J<sub>P-H</sub> 694-700 Hz)<sup>S16</sup> and measurements where phosphonic acid was added to photolyzed **2** (data not shown). The second product (<sup>31</sup>P  $\delta$  = -4.1 ppm) was not identified, but could possibly be MesP(=O)(OH)<sub>2</sub> (**2d**, Scheme S5), as detected by ESI-MS (Fig. S19).

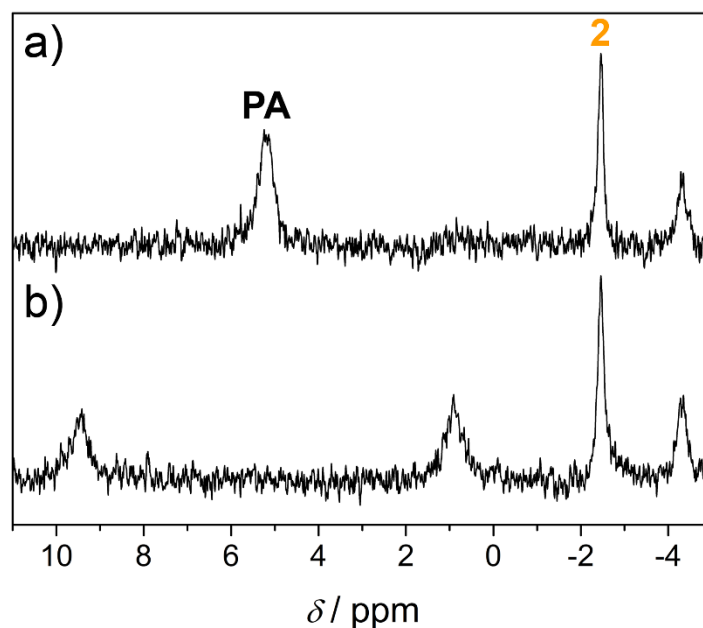


**Fig. S17** a) <sup>1</sup>H decoupled and b) <sup>1</sup>H coupled <sup>31</sup>P NMR spectrum of BAPO-OH (**2**) in acetonitrile after photolysis (Hg-Xe lamp,  $\lambda_{\text{max}} = 365$  nm).

## 5.2 ESI-MS of BAPO (1) and BAPO-OH (2) after photolysis

The ESI-MS spectrum (negative mode) of photolyzed **1** is depicted in Fig. S18. Photoproduct **1a** results from the cleavage of one mesityl group (**M**) and the addition of a hydroxyl group (Scheme S5). A comparison of the experimental and the theoretical exact mass is listed in Table S13. Phenylphosphinic acid –  $[\text{C}_6\text{H}_7\text{PO}_2\text{-H}]^-$ ,  $(m/z)^{\text{theo}} = 141.0105$  – was not detected.

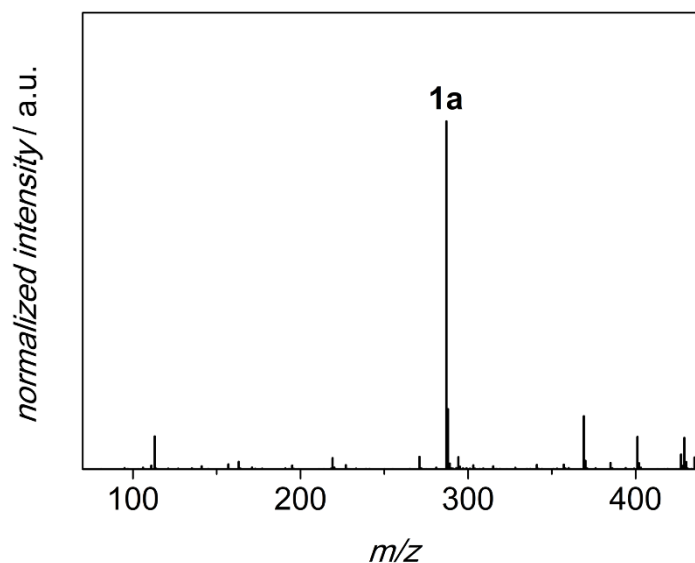


**Fig. S18** ESI-MS spectrum (negative mode) of BAPO (**1**; 5 mM in acetonitrile) after photolysis ( $\lambda = 351$  nm, 1.5 mJ/pulse, 200 Hz, 10,000 pulses).

**Table S13** Assigned Signal after the Photolysis ( $\lambda = 351$  nm, 1.5 mJ per Pulse, 200 Hz, 10,000 Pulses) of BAPO (**1**; 5 mM in acetonitrile), as Detected by ESI-MS (Negative Mode)

Label	Compound	Formula	$(m/z)^{\text{exp}}$	$(m/z)^{\text{theo}}$	$\Delta(m/z)$
<b>1a</b>	MesP(=O)(Ph)OH	$[\text{C}_{16}\text{H}_{17}\text{PO}_3\text{-H}]^-$	287.0842	287.0837	0.0005

The ESI-MS spectrum (negative mode) of photolyzed **2** is depicted in Fig. S19. The assigned signals are listed in Table S14 and the structures are shown in Scheme S5. Phosphonic acid ( $\text{H}_3\text{PO}_3$ , **2a**) was detected in its dimeric (**2b**) and trimeric form (**2c**) and as adduct with photoproducts (**2e**) and residual BAPO-OH **2** (**2g**).

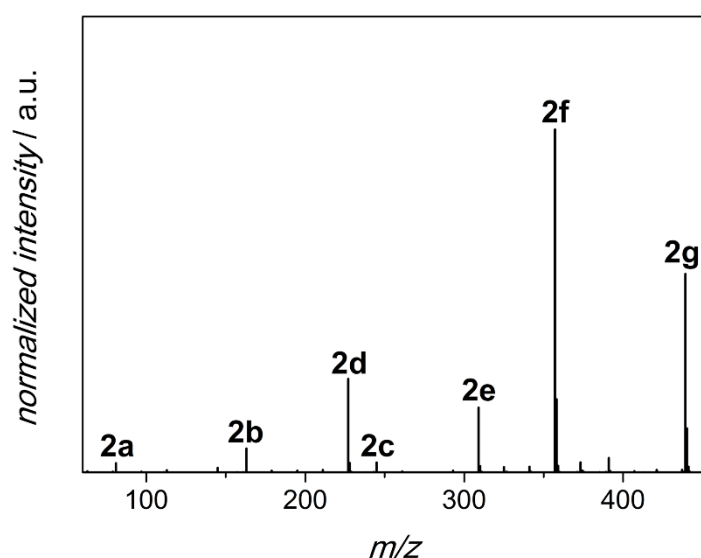
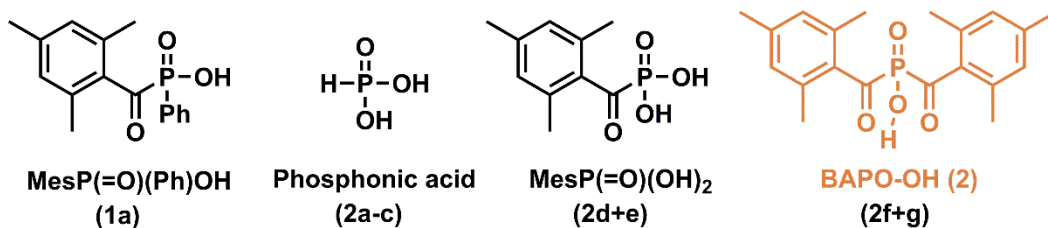


**Fig. S19** ESI-MS spectrum (negative mode) of BAPO-OH (**2**; 5 mM in acetonitrile) after photolysis ( $\lambda = 351$  nm, 1.5 mJ/pulse, 200 Hz, 10,000 pulses).

**Table S14** Overview of the Assigned Signals after the Photolysis ( $\lambda = 351$  nm, 1.5 mJ per Pulse, 200 Hz, 10,000 Pulses) of BAPO-OH (**2**; 5 mM in Acetonitrile), as Detected by ESI-MS (Negative Mode)

Label	Compound	Formula	$(m/z)^{\text{exp}}$	$(m/z)^{\text{theo}}$	$\Delta(m/z)$
<b>2a</b>	Phosphonic acid	$[\text{H}_3\text{PO}_3\text{-H}]^-$	80.9732	80.9742	0.0010
<b>2b</b>	Phosphonic acid dimer	$[\text{H}_6\text{P}_2\text{O}_6\text{-H}]^-$	162.9556	162.9561	0.0005
<b>2c</b>	Phosphonic acid trimer	$[\text{H}_9\text{P}_3\text{O}_9\text{-H}]^-$	244.9384	244.9381	0.0003
<b>2d</b>	MesP(=O)(OH) <sub>2</sub>	$[\text{C}_{10}\text{H}_{13}\text{PO}_4\text{-H}]^-$	227.0474	227.0473	0.0001
<b>2e</b>		$[\text{C}_{10}\text{H}_{13}\text{PO}_4\text{+H}_3\text{PO}_3\text{-H}]^-$	309.0298	309.0293	0.0005
<b>2f</b>	BAPO-OH ( <b>2</b> )	$[\text{C}_{20}\text{H}_{23}\text{PO}_4\text{-H}]^-$	357.1259	357.1256	0.0003
<b>2g</b>		$[\text{C}_{20}\text{H}_{23}\text{PO}_4\text{+H}_3\text{PO}_3\text{-H}]^-$	439.1079	439.1076	0.0003



**Scheme S5** Products of the Photolysis ( $\lambda = 351$  nm, 1.5 mJ per Pulse, 200 Hz, 10,000 Pulses) of BAPO (**1**) and BAPO-OH (**2**), as Detected by ESI-MS (Negative Mode).

## 6 Femtosecond Pump Probe Spectroscopy

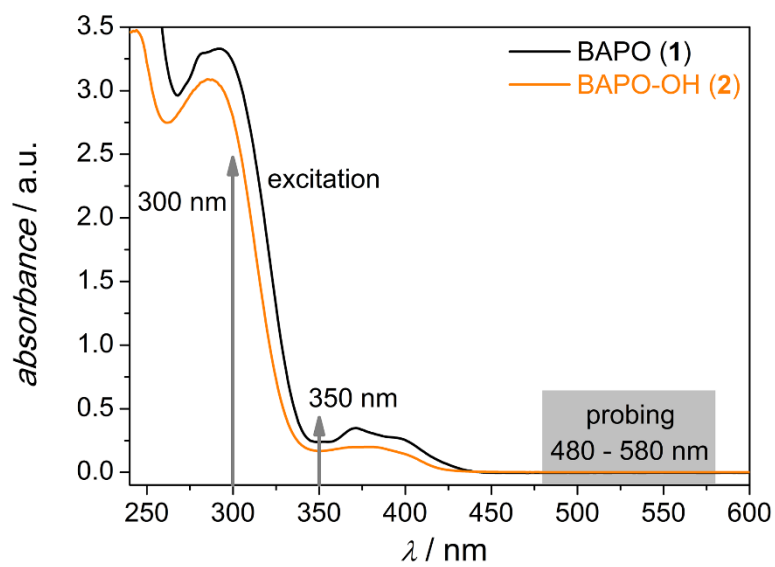


**Fig. S20** UV/Vis spectra of BAPO (1) and BAPO-OH (2) in methyl isobutyrate and depiction of the excitation (300 and 350 nm) and probing wavelengths (480 – 580 nm).

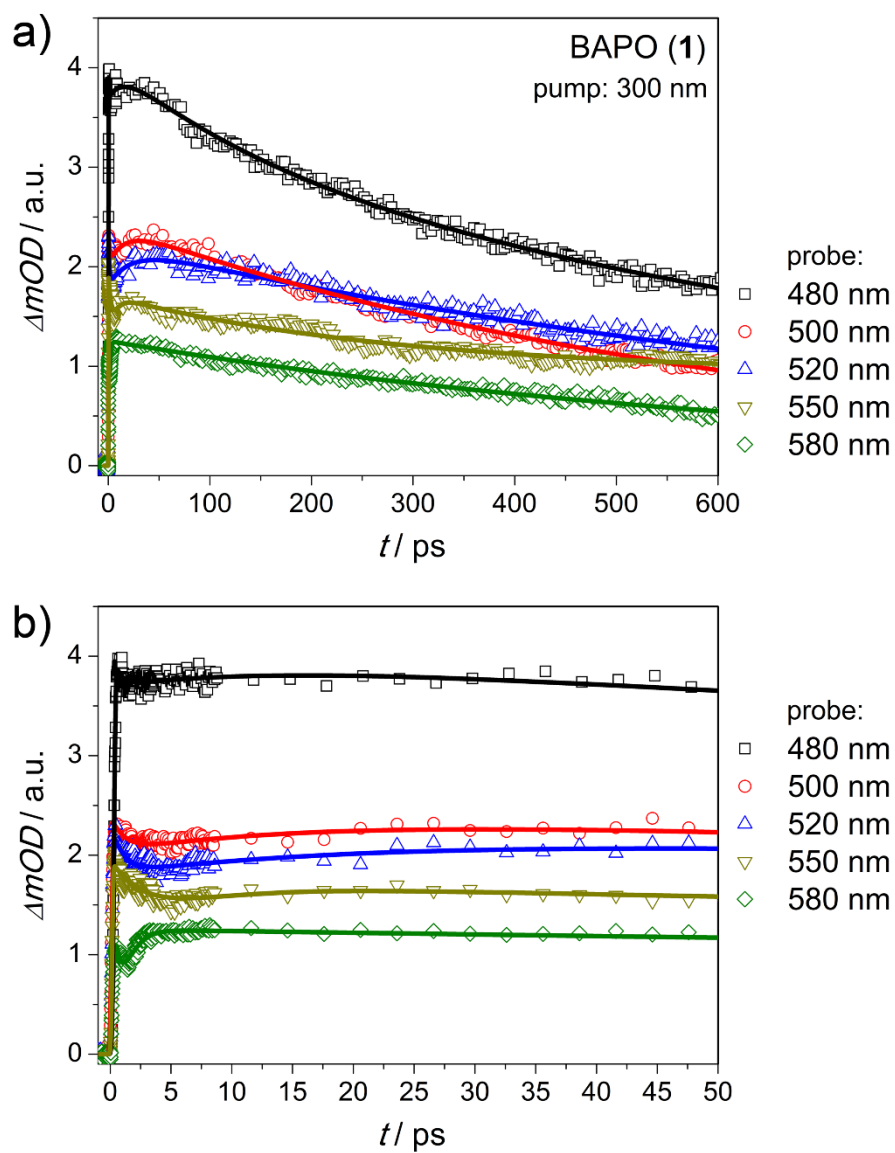


**Fig. S21** a) Transient absorption of BAPO (1) in methyl isobutyrate solution pumped at 300 nm and probed at 480 to 580 nm, and b) zoom into the first 50 ps. Lines are to guide the eye.

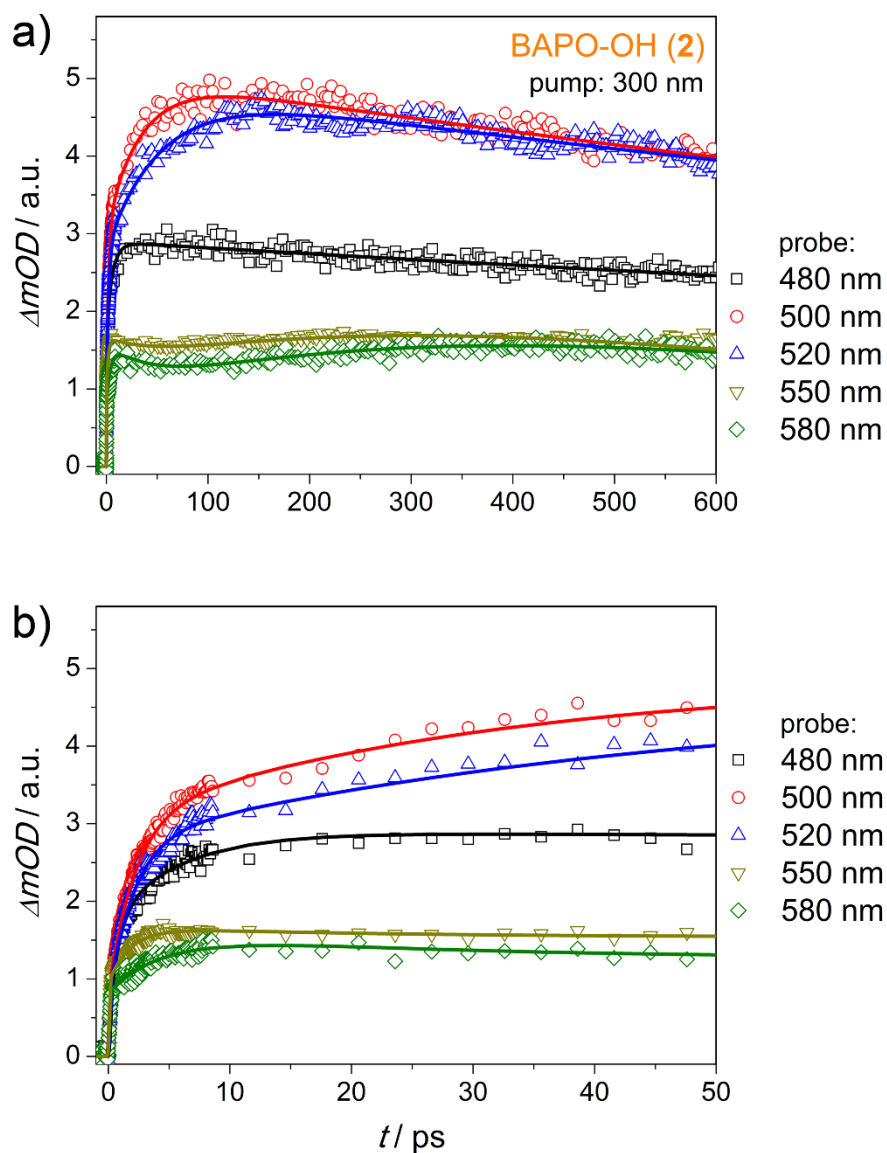


**Fig. S22** a) Transient absorption of BAPO-OH (**2**) in methyl isobutyrate solution pumped at 300 nm and probed at 480 to 580 nm, and b) zoom into the first 50 ps. Lines are to guide the eye.

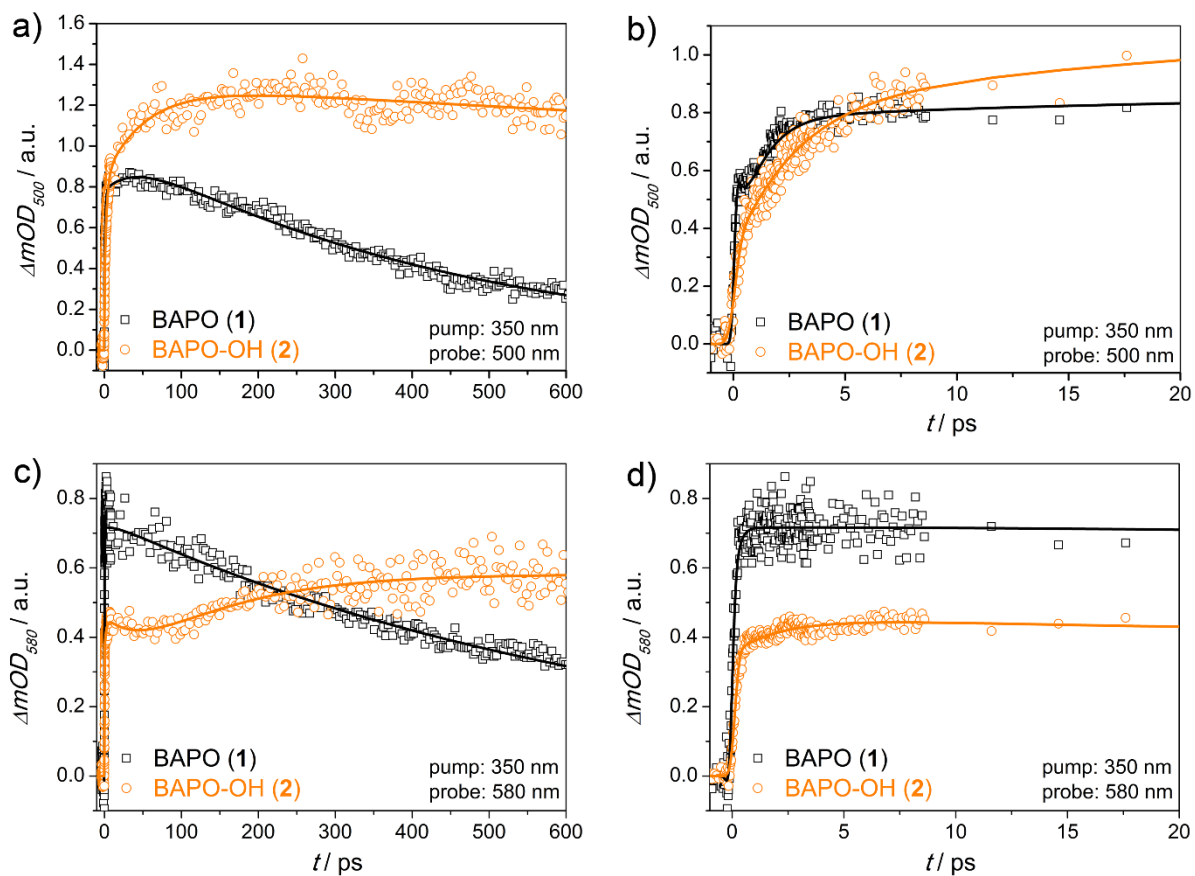


**Fig. S23** Transient absorptions of BAPO (1) and BAPO-OH (2) in methyl isobutyrate pumped at 350 nm and probed at a+b) 500 nm and c+d) 580 nm.



## 7 References

- S1 WO 2014095724A1, 2014.
- S2 G. Müller, M. Zalibera, G. Gescheidt, A. Rosenthal, G. Santiso-Quinones, K. Dietliker, H. Grützmacher, *Macromol. Rapid Commun.*, 2015, **36**, 553-557.
- S3 T. J. A. Wolf, D. Voll, C. Barner-Kowollik and A.-N. Unterreiner, *Macromolecules*, 2012, **45**, 2257–2266.
- S4 A. D. Becke, *J. Chem. Phys.*, 1993, **98**, 5648-5652.
- S5 C. Lee, W. Yang and R. G. Parr, *Phys. Rev. B*, 1988, **37**, 785–789.
- S6 P. J. Stephens, F. J. Devlin, C. F. Chabalowski and M. J. Frisch, *J. Phys. Chem.*, 1994, **98**, 11623–11627.
- S7 F. Weigend and R. Ahlrichs, *Phys. Chem. Chem. Phys.*, 2005, **7**, 3297–3305.
- S8 T. Yanai, D. P. Tew and N. C. Handy, *Chem. Phys. Lett.*, 2004, **393**, 51–57.
- S9 A. Schäfer, C. Huber and R. Ahlrichs, *J. Chem. Phys.*, 1994, **100**, 5829–5835.
- S10 F. Neese, F. Wennmohs and A. Hansen, *J. Chem. Phys.*, 2009, **130**, 114108.
- S11 F. Neese, *Wiley Interdiscip. Rev.: Comput. Mol. Sci.*, 2012, **2**, 73–78.
- S12 M. Kumar, D. H. Busch, B. Subramaniam and W. H. Thompson, *J. Phys. Chem. A*, 2014, **118**, 9701–9711.
- S13 A. Klamt and G. Schüürmann, *J. Chem. Soc., Perkin Trans. 2*, 1993, 799–805.
- S14 A.-R. Allouche, *J. Comput. Chem.*, 2011, **32**, 174–182.
- S15 M. Griesser, D. Neshchadin, K. Dietliker, N. Moszner, R. Liska and G. Gescheidt, *Angew. Chem., Int. Ed.*, 2009, **48**, 9359–9361.
- S16 M. J. Gallagher, in *Handbook of Phosphorus-31 Nuclear Magnetic Resonance Data*, ed. J. C. Tebby, CRC Press, Boston, 1991, ch. 10, pp. 287-296.
- S17 M. A. El-Sayed, *J. Chem. Phys.*, 1963, **38**, 2834-2838.
- S18 A.-M. Kelterer, G. Uray and W. M. F. Fabian, *J. Mol. Model.*, 2014, **20**, 2217.